In vivo screening reveals cell-intrinsic mediators of solid tumor resistance to CAR T cell-therapy

Julia Fröse[1,2*], Charles A. Whittaker[1], Paul Leclerc[1,2], Evelyn Chen[1,2], Sean Doherty[1,2], Adam Langenbucher[1,2], Riley D. Hellinger[1,2], Daniel Goulet[1,2], Tuomas Tammela[3,4], Michael T. Hemann[1,2*]

Affiliations:
[1] The David H. Koch Institute for Integrative Cancer Research; Cambridge, MA 02142, United States
[2] Department of Biology, Massachusetts Institute of Technology; Cambridge, MA 02142, United States
[3]Cancer Biology and Genetics Program, Sloan Kettering Institute, Memorial Sloan Kettering Cancer Center, New York, New York
[4]David M. Rubenstein Center for Pancreatic Cancer, Memorial Sloan Kettering Cancer Center, New York, New York

*Corresponding authors. Email: jfroese@mit.edu, hemann@mit.edu

Abstract

Chimeric antigen receptor (CAR) T-cell therapy has transformed the treatment of hematologic cancers. However, its efficacy in solid tumors, including pancreatic ductal adenocarcinoma (PDAC), has been limited. By integrating modular CRISPR screening with immunocompetent orthotopic models of PDAC, we identified unknown tumor-intrinsic modulators of CAR T-cell therapy response. Disruption of genes involved in oxidative and proteotoxic stress, particularly the Nrf2 target *Slc33a1*, sensitizes PDAC tumors to CAR T-cell killing. Single cell gene expression analyses revealed that CAR-T resistant tumors exhibit reduced Nrf2 pathway activity. Mechanistically, we show that Nrf2 pathway hyperactivation by genetic ablation of *Keap1* or expression of a tumor-derived *Keap1* allele sensitized PDAC tumors to CAR T-cell therapy. Thus, cell-intrinsic molecular states accompanying malignant progression can sensitize tumor cells to cell-based immunotherapies. These molecular mechanisms could be exploited to augment both the efficacy of CAR-T cell therapy in solid malignancies, and may allow patient stratification by tumor genotype.

Statement of significance

CAR T-cell therapy remains an unsolved challenge for pancreatic cancer. The discovery of tumor-intrinsic mechanisms of resistance has been largely limited by current experimental models. Using large-scale genomic screening in an orthotopic, immunocompetent model of pancreatic cancer, we uncover a role for cell-intrinsic metabolic states in regulating CAR T-cell response.

Introduction

Pancreatic ductal adenocarcinoma (PDAC) is projected to become the second leading cause of cancer death by 2030[1,2]. PDAC lacks effective treatment options, and innovative strategies for therapeutic intervention are urgently needed[3]. The use of chimeric antigen receptor (CAR) T-cell therapy, in which a patient's own T cells are engineered to recognize and kill cancer cells, has shown remarkable success in recent years in hematological malignancies[4–6]. The adaptation of these therapies to solid tumors such as pancreatic cancer holds great promise[7]. However, clinical trials for CAR T-cell therapy in PDAC have shown limited efficacy in patients[8]. As of now, no universal mechanism underlying the success or failure of these therapies has been discovered.

CAR T-cells face a host of challenges, especially in solid tumor microenvironments, such as inefficient homing to the tumor site, immunosuppressive tumor microenvironments, and lack of persistence in the tumor due to exhaustion or other factors[9–11]. Many strategies for improving CAR T-cell therapy efficacy have focused on further engineering CAR T-cells to improve their persistence and expansion or prevent exhaustion in cancer patients[12–17]. However, initial studies examining tumor response to immune checkpoint blockade have shown that tumor cell-intrinsic properties can also play important roles in influencing the response to immunotherapy[18]. Recent studies have identified tumor-intrinsic mechanisms of CAR T-cell therapy resistance and disease relapse, including antigen loss on tumor cells[19–21], impaired death receptor signaling in tumor cells[22], and alterations in the IFN-γ pathway[23–26]. Nevertheless, to date, no cancer-specific dependencies have been discovered that can influence CAR T-cell therapy response. It also remains unclear whether the spectrum of cancer alterations that underlie tumor responses to conventional or targeted chemotherapy can similarly impact response to CAR-T treatment.

Solid tumors are complex ecosystems of tumor cells, as well as multiple types of infiltrating immune cells, fibroblasts, and endothelial cells[27]. PDAC tumors are particularly complex malignancies characterized by substantial inter- and intertumoral heterogeneity, as well as an unusually dense fibrotic stroma. Recent studies have also shown that PDAC

tumors harbor distinct phenotypic states, including classical, basal, and mesenchymal states[28–30]. Additionally, different cell states have been shown to modulate response to targeted therapies and cytotoxic T cell killing[31,32].

A number of studies focused on CAR T-cell therapy resistance in solid tumors have relied on CRISPR-Cas9 knockout (KO) screens in cell culture, immunodeficient mouse models, or heterotopic locations [26,33]. While these screens have uncovered important biology, *in vivo* screening in orthotopic locations and in the presence of a fully functional immune system may reveal previously unknown tumor-intrinsic mediators of CAR T-cell response. Understanding which tumor-intrinsic mechanisms mediate resistance to immunotherapy in relevant physiological settings is key in designing effective treatments for patients.

To uncover tumor cell-intrinsic mechanisms of resistance to CAR T-cell therapy in PDAC, we performed iterative CRISPR-Cas9-based pooled KO screens in a fully immunocompetent, orthotopic model of PDAC treated with CAR T-cells. In this physiological setting, we uncovered previously unknown modulators of CAR T-cell therapy response. We found that loss of genes involved in redox homeostasis and proteotoxic and oxidative stress, particularly *Slc33a1* and *Sptlc1*, is sufficient to sensitize PDAC tumors to CAR T-cell treatment *in vivo*. Importantly single-cell RNA sequencing (scRNA seq) of CAR T-cell-treated PDAC tumors that therapy-resistant tumor cells exhibit a metabolic cell state characterized by reduced antioxidant pathway activation, reactive oxygen species (ROS) signaling, and glutathione metabolism. Mechanistically, we show that hyperactivation of the Keap1/Nrf2 antioxidant response pathway by genetic ablation of *Keap1* or expression of a tumor-derived *Keap1* allele is sufficient to sensitize PDAC tumors to CAR T-cell therapy. Our data indicate a potential avenue for therapeutic synergy by targeting pathways involved in oxidative stress to increase the efficacy of CAR T-cell therapy in PDAC. More broadly, our work presents a general strategy to integrate functional genomics with pre-clinical mouse models to study mechanisms of response and resistance to state-of-the-art cell-based immunotherapies.

Results

A scalable mouse model of PDAC to study CAR T-cell therapy resistance

To identify genetic mediators of the response to CAR T-cell therapy in an unbiased manner, we established a murine PDAC model that allows for large scale CRISPR KO screens and is targetable by murine CAR-T cells. For this purpose, a PDAC cell line established from autochthonous pancreatic tumors arising in the KPC (*LSL-Kras*$^{G12D/+}$*;LSL-Trp53*$^{R172H/+}$*;Pdx1-Cre*) mouse model (**Figure 1A**) was engineered to express both *Firefly luciferase* (Luc) and *Sp. Cas9*[34]*.* A Cas9-expressing (Cas9+) PDAC cell clone with high Cas9 cleavage efficiency (**Figure S1A-B**) was established. This clone was further modified to express human CD19 (hCD19) without the intracellular domain, as an antigen for CAR T-cell treatment (hCD19+ PDAC; **Figure S1C**). We used CD19 as a tumor antigen for three reasons. First, it allowed us to use established human anti-CD19 CARs. Second, it narrowed the potential scope of biology emerging from the screen results by eliminating the relevance of genes involved in endogenous antigen presentation. Third, this strategy can be extrapolated to other tumor types that may lack suitable murine CAR T-cell targets.

To determine whether *in vivo* screens with hCD19+ PDAC using immunocompetent mouse cells are feasible, we examined the growth kinetics and tumor volumes of both Luc+ PDAC cells and hCD19+ PDAC cells. These cells exhibit similar *in vitro* proliferation rates (**Figure S1D**). Tumor growth kinetics were also similar between Luc+ and hCD19+ PDAC cells over a time course of 10 days, indicating that engineered PDAC cells exhibit no or very little immunogenicity *in vivo* (**Figure S1E**). Furthermore, we did not observe any differences in the weight of orthotopic PDAC tumors established from Luc+ or hCD19+ PDAC cells in either immunocompetent C57BL/6 mice or immunodeficient NOD-SCID/IL2Rg−/− (NSG) mice (**Figure S1F-G**). This lack of immunogenicity is in line with previously published work using a Cas9+ murine B cell acute lymphoblastic leukemia (B-ALL) model in C57BL/6 mice[23].

Next, we investigated whether hCD19+ PDAC cells are susceptible to CAR T-cell killing *in vitro*. We incubated 10,000 hCD19+ PDAC cells with increasing effector-to-target (E:T)

ratios of murine CAR T-cells targeting EGFRvIII, a control Ag not expressed by our cells, or the model antigen hCD19 for 24 hours (**Figure 1B**). We observed efficient killing of PDAC cells at all E:T ratios tested (5:1, 10:1 and 20:1), as well as a strong release of IFN-γ by hCD19 CAR T-cells compared to control CAR T-cells (**Figure 1C**).

To test whether hCD19+ PDAC cells could also be targeted by CAR T-cells *in vivo*, we transplanted 600,000 hCD19+ PDAC cells orthotopically into the pancreas of fully immunocompetent C57BL/6 mice followed by intraperitoneal injection of 2.5 million murine control or hCD19 CAR T-cells four days later (**Figure 1D**). Tumor growth, monitored by ultrasound over the following ten days, was significantly delayed in mice treated with hCD19 CAR T-cells compared to controls (**Figure 1E**), and this translated into a survival benefit (**Figure 1G**). Despite continued tumor enlargement during treatment, histological analysis revealed extensive necrosis, hemorrhage, and dense immune cell infiltration in CAR T-cell–treated tumors (**Figure S1H**), consistent with robust intratumoral CAR T-cell activity.

Having established that hCD19+ PDAC cells can be targeted by hCD19 CAR T-cells *in vivo*, we then tested whether CAR T-cell treatment can provide the selective pressure required to successfully identify mediators of response and resistance using CRISPR-Cas9 KO screening. To do so, we first knocked out the hCD19 antigen in hCD19+ PDAC cells using multiple sgRNAs followed by combining KO cells with mock -negative PDAC cells (**Figure S2A**). Next, we mixed antigen-positive (GFP+) PDAC cells with antigen-negative (E2-Crimson+) PDAC cells at a 50:50 ratio and treated them with control (EGFRvIII) or hCD19 CAR T-cells at an E:T ratio of 10:1 for 24 hours *in vitro* (**Figure S2B**). Treatment with hCD19 CAR T-cells, but not control CAR T-cell treatment or no treatment, led to an increase in antigen-negative PDAC cells relative to antigen-positive PDAC cells (**Figure S2C**). Similarly, orthotopic injection of a 50:50 mixture of antigen-positive (GFP+) and antigen-negative (E2-Crimson+) PDAC cells followed by CAR T-cell treatment with hCD19 or control CAR T-cells lead to an enrichment of antigen-negative PDAC cells over a period of 10 days (**Figure 1H-I**). Together, these results demonstrate that a genetic alteration conferring CAR T-cell resistance can be enriched and successfully identified both *in vitro* and *in vivo*.

For successful *in vivo* CRISPR-Cas9 KO screening, it is essential to maintain an adequate representation of single guide RNAs (sgRNAs) throughout the experiment[35]. The size limit of the sgRNA library that can be screened robustly *in vivo* is influenced by the tumor type, the number of tumor cells that can be safely injected, and the engraftment efficiency of tumor cells in the chosen location. To empirically determine the maximum library size that can be screened in the hCD19+ PDAC model, we generated individual hCD19+ PDAC cell lines expressing either GFP+ or mCherry+ to perform limiting GFP-dilution assays *in vivo*. To do so, we established five groups of hCD19+ PDAC cells containing diminishing amounts of GFP+ hCD19+ PDAC cells (50%, 1%, 0.1%, 0.05%, or 0.025%) mixed with mCherry+ hCD19+ PDAC cells. Next, a total of 600,000 hCD19+ PDAC cells were orthotopically transplanted into C57BL/6 mice (**Figure S2D**). Each GFP percentage corresponds to the maximal empirical library size that could be used if the corresponding GFP percentage was recovered at the experimental endpoint (**Figure S2E**). Ten days after transplantation, PDAC tumors were isolated and analyzed by flow cytometry for GFP+ PDAC cells. We then compared the percentage of GFP+ cells recovered at the end-point ("output") to the starting percentage of GFP+ cells prior to orthotopic transplantation ("input") (**Figure S2F**). In all experimental groups, the empirical output to input ratio was ~1, indicating robust *in vivo* maintenance of GFP+ PDAC cells throughout the entire experiment. These results indicate that our hCD19+ PDAC model could adequately represent a library of ~4000 sgRNAs at 150x coverage *in vivo*. Taken together, we have established an immunocompetent, orthotopic PDAC model amenable to CRISPR-Cas9 KO screening in the context of CAR T-cell therapy.

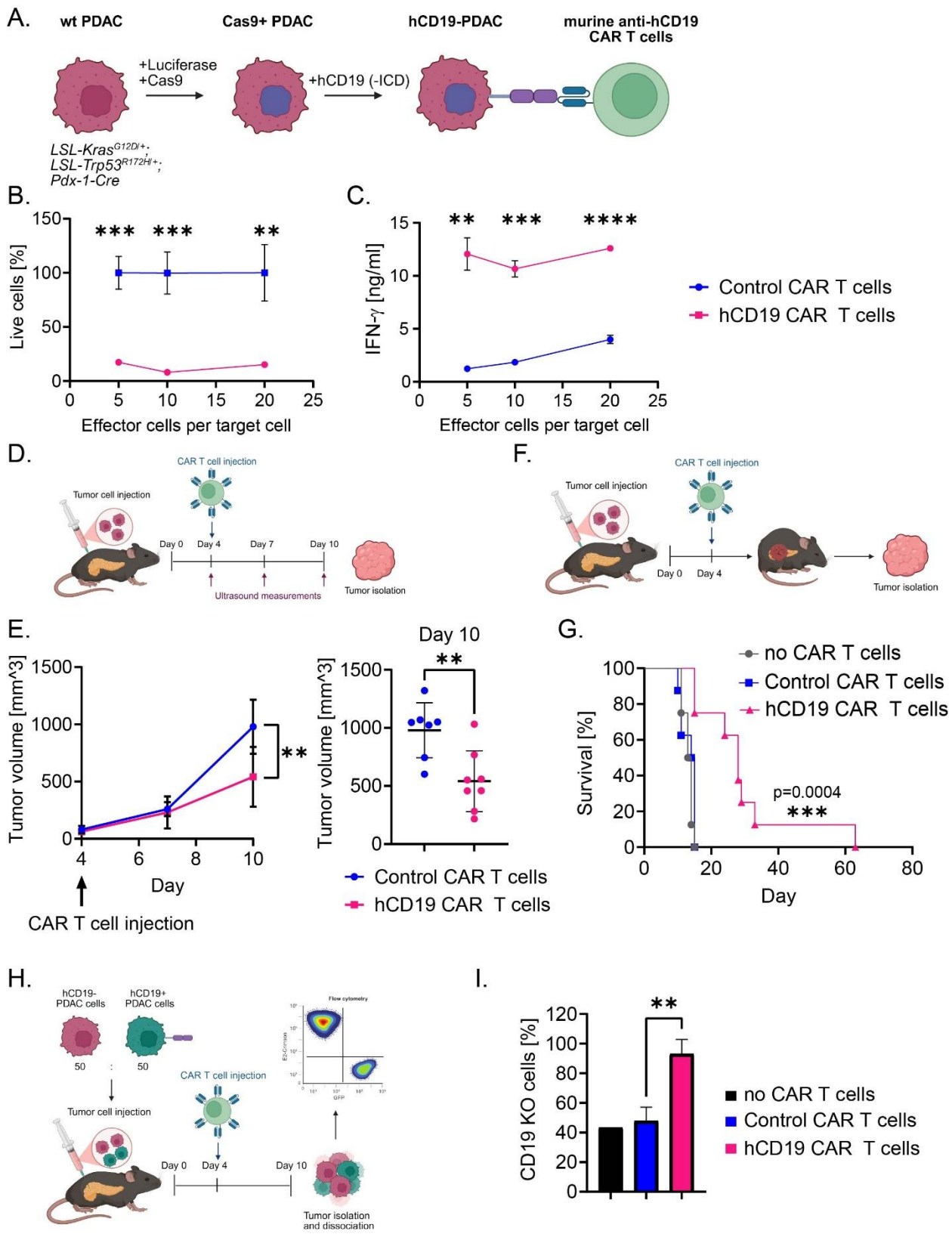

Figure 1: Development of a CRISPR-Cas9 knock-out screening-amenable PDAC model for studying CAR T-cell therapy resistance. A) A KPC (*LSL-Kras*$^{G12D/+}$*;LSL-Trp53*$^{R172H/+}$*;Pdx1-Cre*) tumor-derived

murine PDAC cell line was engineered to stably express *Firefly Luciferase*, *Sp. Cas9*, and hCD19, with a deletion of the intracellular domain (-ICD). The final cell line was established from a single cell cloned to ensure uniform Cas9 activity and CAR T-cell antigen expression. **B)** A graph showing a CAR T-cell cytotoxicity assay involving incubation of hCD19 CAR T-cells or control (anti-EGFRvIII) CAR T-cells with hCD19+ PDAC cells at multiple effector-to-target ratios (E:T ratios = CAR T-cells:PDAC cells = 5:1, 10:1, 20:1) for 24 hours. All conditions were analyzed in triplicates and error bars represent standard deviation. Statistical analysis was conducted using unpaired t-test. **C)** A graph showing the level of IFN-γ release from hCD19 or control CAR T-cells during the CAR T-cell assay. All conditions were analyzed in triplicate and error bars represent standard deviation. Statistical analysis was conducted using unpaired t-test (ns > 0.05, * ≤ 0.05, ** p ≤ 0.01, *** p ≤ 0.001, **** p ≤ 0.0001). **D)** Experimental schematic: C57BL/6 mice received an orthotopic injection of 600,000 hCD19+ PDAC cells, followed by a subsequent intraperitoneal injection of freshly prepared hCD19 CAR T-cells (n=8; 2.5 million) or control irrelevant CAR T-cells (n=7) four days later. Tumor volume was measured every 3 days using ultrasound. **E)** (Left) A graph showing the tumor volume following CAR-T treatment. (Right) On day 10, hCD19+ PDAC tumors treated with hCD19 CAR-T cells are significantly (p=0.0059) smaller than control CAR T-cell treated tumors. Error bars represent standard deviation. Statistical analysis was conducted using a Mann-Whitney test. **F)** Experimental schematic: C57BL/6 mice received an orthotopic injection of 600,000 hCD19+ PDAC cells, followed by a subsequent intraperitoneal injection of freshly prepared hCD19 CAR T-cells (n=8; 2.5 million) or control irrelevant CAR T-cells (n=8), or no CAR T-cells four days later (n=8). Mice were monitored until a humane endpoint was reached and their survival was recorded. **G)** A Kaplan-Meier curve showing overall survival of mice bearing hCD19+ PDAC tumors treated with hCD19 CAR T-cells, not treated or treated with control CAR T-cells. CAR-T treatment significantly extends survival compared to treatment with control CAR T-cells (Mantel-Cox test p=0.0004). **H)** Experimental schematic: PDAC cells with (GFP+) and without the hCD19 antigen (E2-Crimson+) were mixed at a 50:50 ratio. A total of 600,000 PDAC cells was orthotopically injected into C57BL/6 mice, followed by a subsequent intraperitoneal injection of freshly prepared hCD19 CAR T-cells (n=5; 2.5 million) or control irrelevant CAR T-cells (n=5) four days later. After ten days, PDAC tumors were isolated, dissociated into single cells, and analyzed by flow cytometry for GFP+ and E2-Crimson+ tumor cells. **I)** A bar graph showing that PDAC tumor cells without the CD19 antigen (E2-Crimson+) enrich over time in CAR T-cell treated PDAC tumors. Error bars represent standard deviation. Statistical analysis was conducted using a Mann-Whitney test (p=0.0079).

In vivo CRISPR-Cas9 screens reveals modulators of CAR T-cell response in PDAC

Next, we performed iterative KO screens using the hCD19+ PDAC model system to uncover genetic modulators of CAR T-cell response in pancreatic cancer. For this purpose, we made use of the modular SKY CRISPR library that is divided into non-redundant pools that can be individually screened or combined into larger libraries[23]. All protein-coding murine genes in this genome-wide library, with four sgRNAs per gene, were divided into 48 pools. Using their initial Kyoto Encyclopedia of Genes and Genomes (KEGG) term in a non-redundant manner, 36% of protein-coding genes could be classified into a KEGG pathway. This led to the first 14 pools and part of pool 15 covering all KEGG pathways. All other genes were randomly distributed among the remaining pools. Each pool also contained control sgRNAs targeting intergenic regions, olfactory

genes, and murine essential genes[36]. Additionally, guides against human CD19 were included in the first pool.

We performed a total of eight independent KO screens covering the first 16 pools of the SKY library (**Table S1**). Guided by our limiting dilution experiments (**Figure S2E-F**), we decided to combine and screen two library pools (~3800 total sgRNAs) in individual mice. Each screen was performed by transplanting 600,000 sgRNA-expressing hCD19+ PDAC cells orthotopically into the pancreas of C57BL/6 mice followed by treatment with murine hCD19 CAR T-cells or control CAR T-cells targeting EGFRvIII four days later (**Figure 2A**). Each batch of freshly produced murine CAR T-cells was functionally tested for antigen-dependent on-target killing efficiency and IFN-γ release in cytotoxicity assays *in vitro* before using them for *in vivo* screens (**Figure S3A-C**). Tumors were isolated between 10 and 25 days after initial injection, which was when mice showed advanced tumor burden (**Figure S3D-K**). Each tumor was then dissociated into single cell suspensions and subjected to high-throughput sequencing to quantify sgRNA representation. sgRNA coverage was well maintained in all tumors harvested from each experimental arm compared to pre-screen input samples (**Figure S4A-B**). To further assess screen quality, we confirmed that sgRNAs targeting essential genes were significantly depleted in both the control and hCD19 CAR T-cell treated groups, whereas those targeting non-essential genes did not (**Figure S5A**). These results highlight the robustness of our screens.

Next, we used the Model-based Analysis of Genome-wide CRISPR-Cas9 Knockout (MAGeCK) algorithm to analyze the sequencing data from all screens (**Figure 2B**)[37]. Both the MAGeCK FluteRRA and FluteMLE algorithms were used to determine significantly enriched or depleted sgRNAs between control CAR T-cell treated and hCD19 CAR T-cell treated PDAC tumor cells. In the resulting data, enriched sgRNAs are predicted to target genes whose inactivation mediates resistance to CAR T-cell therapy, while depleted sgRNAs target genes whose loss sensitizes PDAC cells to CAR T-cell therapy. Genes were considered a “hit” if they fulfilled four rigorous criteria: (1) a log-fold change (LFC) of greater than 1.3 or smaller than -1.3 (as determined by FluteRRA) or a beta score higher than 12 (as determined by FluteMLE), (2) a False Discover Rate (FDR) equal to or smaller

than 0.1, (3) at least two out of four guide RNAs changing in the same direction, and (4) not part of the essential gene catalog defined by Hart *et al*[36]. Importantly, sgRNAs targeting the hCD19 CAR T-cell antigen showed the strongest enrichment of all sgRNAs in the first screen (**Figure 2C**). These results confirm that adequate selective pressure was generated with CAR T-cell therapy in our hCD19+ PDAC model, allowing us to identify genetic modulators of CAR T-cell response *in vivo*. Across all eight KO screens, a total of 244 genes fulfilled our "hit" selection criteria and altered the representation of hCD19+ PDAC cells following CAR T-cell therapy (**Table S2**). Of these 244 potential CAR T-cell therapy modulators, 30 genes were classified as "sensitizers" and the remaining 204 genes were classified as "resistance" genes.

A caveat of our pooled screening approach is that it does not enable a ranked comparison between sgRNAs across separate screens. Therefore, we performed a validation screen using a new CRISPR KO library containing six sgRNAs targeting each gene previously identified as a "hit" (**Table S2**). We also included 90 non-targeting (scrambled) sgRNAs, 213 intergenic cutting control sgRNAs, and 91 olfactory gene-targeting sgRNAs that exhibited neutral behavior (no enrichment or depletion) in our initial screens. We performed this validation screen in an identical fashion to our previous KO screens. As previously, we assayed CAR T-cell functionality by testing their killing efficiency and IFN-γ release in cytotoxicity assays *in vitro* (**Figure S7A-C**). CAR T-cells showed efficient on-target killing and IFN-γ release when exposed to their target antigen. Tumors were isolated when mice showed advanced tumor burden, between 15 and 32 days after initial injection (**Figure S7D**), and sgRNA representation was quantified using high-throughput sequencing. Compared to pre-screen input samples, sgRNA coverage varied between individual PDAC tumors isolated, especially tumors isolated from long-term survivors treated with hCD19 CAR T-cells (**Figure S7E**). As in our primary screens, we observed that sgRNAs targeting known essential genes significantly depleted in both the control and hCD19 CAR T-cell treated groups compared to their respective pre-screen input samples (**Figure S7F**). In contrast, sgRNAs targeting intergenic regions or non-essential genes were unchanged between experimental conditions, confirming screen robustness.

Bona fide modulators of CAR T-cell therapy were determined by assessing the FDR values, log-fold changes, and both intra-screen (within validation screen) and inter-screen (compared to primary screens) consistency of sgRNA behavior (**Figure S7G**). Of the 244 genes that we screened, 30 genes validated as robust modulators of CAR T-cell therapy (**Figure 2D**), and 13 of these were observed to sensitize tumor cells to CAR T-cell therapy as indicated by consistent enrichment of sgRNAs targeting these genes (**Figure 2E**). These genes mainly consisted of known tumor suppressor genes (e.g. *Pten*, *Cdkn2b, Eif4g2*)[38–40], mediators of glycosylation (*Alg10b*, *Alg3*), and genes regulating cell proliferation (e.g. Hippo pathway genes *Nf2, Taok1, Lats2*)[41]. The remaining 17 genes were identified as mediators of resistance to CAR T-cell therapy, as indicated by consistent depletion of sgRNAs targeting those genes (**Figure 2E**). Among these genes, we found mediators of autophagy (*Vmp1, Wrd24*), intracellular trafficking (*Vps29*), and GPI anchoring (*Pigs*), processes that have been previously shown to mediate immune evasion from T cells[42]. We also identified known regulators of clathrin-mediated endocytosis (*Aps2s1, DynII1*) as resistance genes to CAR T-cell therapy[43]. Interestingly, multiple candidate resistance genes are involved in regulating metabolic processes (*Hmgcs1, Sptlc1, Slc33a1, Fxn*)[44–47]. Currently, little is known about the relevance of metabolic pathways for CAR T-cell response, and no alterations in metabolic genes have been described to influence CAR T-cell therapy. This prompted us to interrogate a subset of these genes in depth.

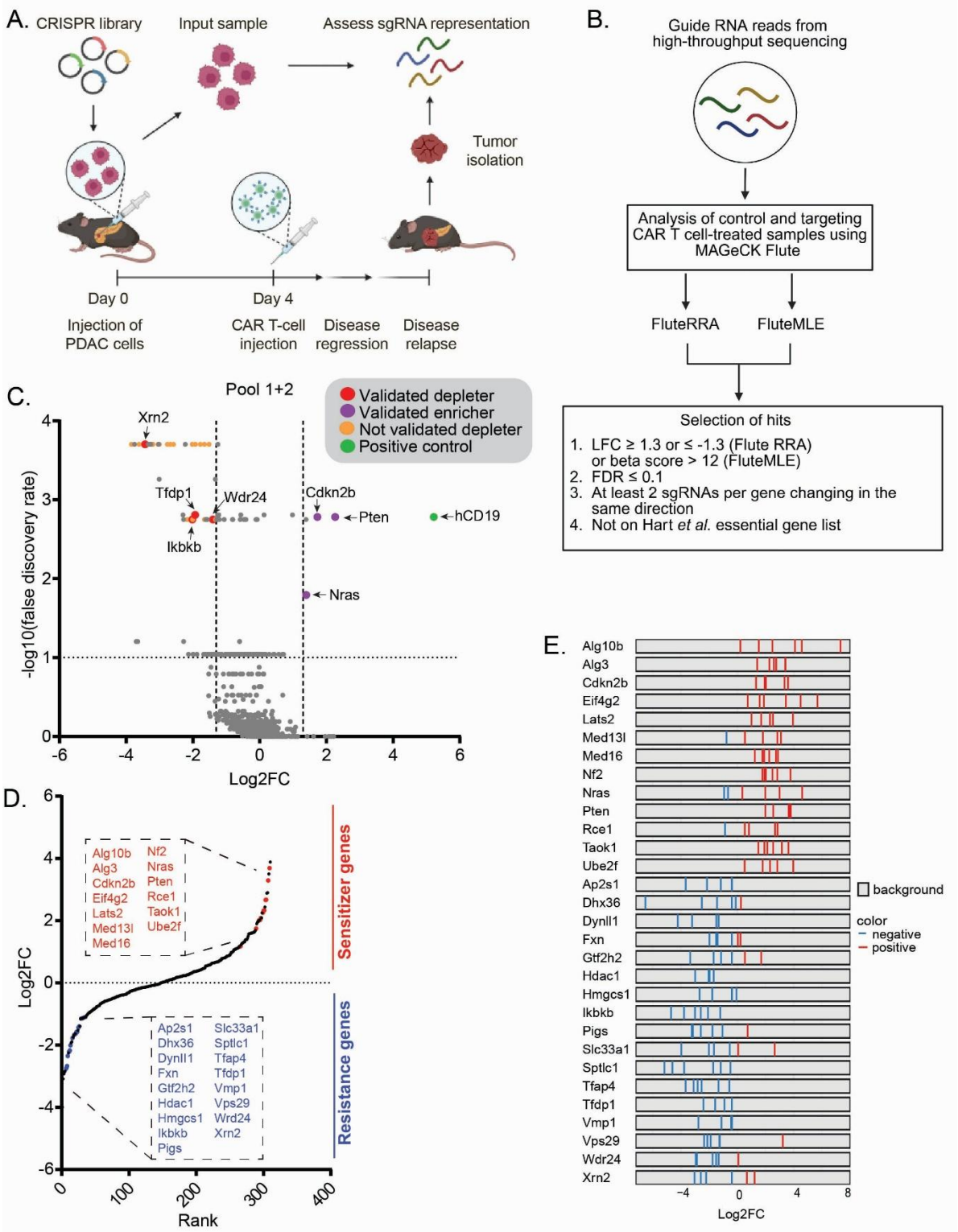

Figure 2: *In vivo* CRISPR-Cas9 KO screening reveals modulators of response to CAR T-cell therapy in PDAC. A) Experimental schematic: murine PDAC cells containing CRISPR library pools were injected orthotopically into C57BL/6 mice, followed by intraperitoneal injection of hCD19 CAR T-cells or control CAR T-cells (n=8 mice per two pools, per CAR T-cell treatment) four days later. Mice were monitored, and tumors were harvested when a humane endpoint was reached. PDAC tumors were dissociated into single cell

suspensions, genomic DNA was isolated and guide RNA representation was determined by next-generation sequencing (NGS). Input samples were harvested of PDAC cells containing the CRISPR libraries on the day of orthotopic injection and also subjected to NGS. In total, eight independent screens were performed, covering more than 6000 genes associated with KEGG pathways. **B)** A schematic of our analysis pipeline: guide RNA reads were analyzed using MAGeCK Flute algorithms. Both the FluteRRA and FluteMLE algorithms were used to determine significantly changed guide RNAs between control CAR T-cell treated and hCD19 CAR T-cell treated PDAC tumor cells. Genes were considered a "hit" if they fulfilled four criteria: (1) an LFC of greater than 1.3 or smaller than -1.3 (FluteRRA) or a beta score higher than 12 (FluteMLE), (2) an FDR equal to or smaller than 0.1, (3) at least two out of four guide RNAs changing in the same direction, and (4) are not considered essential genes (Hart et al.). **C)** A volcano plot showing the results of the first knock-out screen with CRISPR-Cas9 library pools 1 and 2. Library pool 1 contains guide RNAs targeting the CAR T-cell antigen hCD19 as a positive control. "Validated depleter/enricher" refers to genes that were validated in a secondary CRISPR-Cas9 KO screen. "Not validated depleter" refers to genes that were not confirmed as hits in a secondary CRISPR-Cas9 KO screen. **D**) A rank plot (left) of all genes re-screened in a validation CRISPR-Cas9 library under the same conditions described in A. The validation library covers all enrichers and depleters identified in the eight primary CRISPR-Cas9 KO screens and contains six guide RNAs per gene. All genes that validated in this secondary screen are highlighted and listed. In total, 13 genes that promote CAR T-cell response and 17 genes that promote CAR T-cell resistance were identified. **E)** Log2 fold changes of individual guide RNAs for each resistance and sensitizer gene identified in the validation screen. Guide RNA enrichment is shown in red and guide RNA depletion in blue.

Sptlc1 **loss sensitizes PDAC tumors to** ***in vivo*** **CAR T-cell therapy by promoting CAR T-cell infiltration**

Tumor cells exhibit extensive metabolic dysregulation, which can influence their ability to evade immune cells[48]. Interestingly, *Sptlc1* (Serine palmitoyltransferase long chain base subunit 1), a subunit of the serine palmitoyl transferase (Spt) enzyme required for *de novo* sphingolipid biosynthesis[46], has recently been shown to mediate immune evasion in *Kras*-driven cancers[49]. To investigate the influence of *Sptlc1* loss on CAR T-cell therapy, we generated *Sptlc1*-KO clones in Cas9+ PDAC cells (**Figure S8A**). Additionally, we re-expressed a Cas9-resistant version of *Sptlc1* in these KO cells to generate a *Sptlc1* rescue cell line. This Cas9-resistant *Sptlc1* cDNA encodes the identical amino acid sequence as WT *Sptlc1*. We then orthotopically injected C57BL/6 mice with 600,000 PDAC cells containing a *Sptlc1* KO or a control KO (*Olfr402 KO*), followed by injection of 5 million freshly produced murine hCD19 CAR T-cells or control (EGFRvIII) CAR T-cells four days later. We then monitored the mice until a humane endpoint was reached. Consistent with our screen results, both *Sptlc1* KO and control KO PDAC cells formed tumors *in vivo*, and treatment with control CAR T-cells did not lead to any significant difference in survival (**Figure S8B**, left). In contrast, mice injected with *Sptlc1* KO PDAC

cells that were treated with hCD19 CAR T-cells exhibited a statistically significant extension in survival compared to mice injected with control KO PDAC cells. Intriguingly, end-stage tumors isolated from *Sptlc1* KO PDAC mice treated with hCD19 CAR T-cells were significantly larger at morbidity (median survival 18 days) compared to hCD19 CAR T-cell-treated control KO tumors at morbidity (median survival 35 days; **Figure S8B**, right). This suggests that the lethality of *Sptlc1*-deficient tumors is suppressed by CAR-T therapy, and that these tumors are more indolent and able to grow to larger terminal sizes, as mice bearing *Sptlc1* KO tumors live significantly longer without causing morbidity. This is suggestive of pseudoprogression, a clinically observed phenomenon during immunotherapy in which immune-mediated inflammation and cell death lead to apparent increases in tumor volume despite effective antitumor responses[50–52]. In this context, the absence of tumor regression may not reflect therapeutic failure, but rather that tumors reach a size incompatible with survival before meaningful shrinkage can occur. While we cannot definitively distinguish pseudoprogression from true progression in this model, the observed histological changes and survival benefit support this as a potential explanation.

Sptlc1 loss has been shown to lead to a reduction of glycosphingolipids, a major component of the cell membrane, which could alter tumor cell interaction with the immune microenvironment[53]. Therefore, we sought to investigate if *Sptlc1* loss could alter the infiltration of CAR T-cells. We injected C57BL/6 mice with 600,000 PDAC cells containing either a control KO (*Olfr402 KO*), *Sptlc1* KO, or *Sptlc1* rescue and treated with 5 million hCD19 or control CAR T-cells four days later (**Figure S8C**). On day 10, tumors were isolated and analyzed for infiltrating CAR T-cells (GFP+). We found that the amount of infiltrating CAR T-cells was significantly higher in hCD19 CAR T-cell-treated *Sptlc1* KO tumors compared to all other experimental groups (**Figure S8D**). The increased infiltration of antigen-specific CAR T-cells into *Sptlc1* KO tumors could explain the increased life extension seen in mice with *Sptlc1* KO tumors treated with hCD19 CAR T-cells compared to mice with control KO tumors treated with hCD19 CAR T-cells.

To further test if the effect of *Sptlc1* deficiency could be recapitulated with tumor cells expressing a clinically relevant solid tumor antigen, we used wild type (WT) PDAC cells that endogenously express the cell-surface protein mesothelin. Mesothelin has become

an attractive target for cancer immunotherapy due to its limited expression in normal tissues and its high expression in multiple human cancers such as pancreatic, ovarian, and breast cancer. Many clinical trials testing mesothelin (meso)-targeting CAR T-cells in solid tumors are currently underway[54,55]. Therefore, we set out to test whether our WT PDAC cells can be targeted with meso CAR T-cells in an *in vitro* cytotoxicity assay, using a previously developed murine meso (mmeso) CAR construct[56]. We incubated WT PDAC cells with freshly prepared mmeso CAR T-cells at multiple E:T ratios and measured the degree of CAR T-efficacy and IFN-γ release after 24 hours (**Figure S9A-B**). We observed strong dose-dependent killing of WT PDAC cells and potent release of IFN-γ, demonstrating that mmeso CAR T-cells can readily kill PDAC cells *in vitro*.

To further test if the effect of *Sptlc1* deficiency could be recapitulated with tumor cells expressing a clinically relevant solid tumor antigen, we used wild type (WT) PDAC cells that endogenously express the cell-surface protein mesothelin. Mesothelin has become an attractive target for cancer immunotherapy due to its limited expression in normal tissues and its high expression in multiple human cancers such as pancreatic, ovarian, and breast cancer. Many clinical trials testing mesothelin (meso)-targeting CAR T-cells in solid tumors are currently underway[54,55]. Therefore, we set out to test whether our WT PDAC cells can be targeted with meso CAR T-cells in an *in vitro* cytotoxicity assay, using a previously developed murine meso (mmeso) CAR construct[56]. We incubated WT PDAC cells with freshly prepared mmeso CAR T-cells at multiple E:T ratios and measured the degree of CAR T-efficacy and IFN-γ release after 24 hours (**Figure S9A-B**). We observed strong dose-dependent killing of WT PDAC cells and potent release of IFN-γ, demonstrating that mmeso CAR T-cells can readily kill PDAC cells *in vitro*.

Loss of *Slc33a1* sensitizes PDAC tumors to CAR T-cell therapy *in vivo*

Slc33a1, another gene we found to mediate resistance to CAR T-cell therapy, encodes for the solute carrier family member 1 protein, an acetyl-coenzyme A transporter located in the endoplasmic reticulum (ER) membrane[57]. Its function is essential for the lysine acetylation of proteins in the ER, and both loss-of-function or overactivation of *Slc33a1* have been implicated in various diseases[58,59]. In pancreatic acinar cells, *Slc33a1* KO has been shown to result in ER stress, fibrosis, and inflammation[60]. Notably, *Slc33a1*

inactivation was shown to be synthetic lethal with mutation of *Keap1*, a key regulator of the Keap1/Nrf2 antioxidant pathway[61]. To validate *Slc33a1* as a resistance mediator to CAR T-cell therapy, we injected 600,000 hCD19+ PDAC cells with *Slc33a1* KO (**Figure 3A**) or control KO (*Olfr402*) into C57BL/6 mice and treated them with 5 million murine control (EGFRvIII) or hCD19 CAR T-cells four days later (**Figure 3B**). We observed a statistically significant extension of survival in mice injected with *Slc33a1* KO hCD19+ PDAC cells compared to control KO PDAC cells treated with hCD19 CAR T-cells (**Figure 3C**). Mice injected with *Slc33a1* KO hCD19+ PDAC cells treated with hCD19 CAR T-cells ultimately succumbed to disease; however, just like *Sptlc1* KO tumors, end-stage *Slc33a1* KO tumors were significantly larger compared to all other experimental groups and showed extensive immune cell infiltration, hemorrhage, and necrosis (**Figure 3D-E**). These features suggest pseudoprogression[50–52], though we cannot formally distinguish this from true progression in this setting. We also tested whether a mock-bulk population of *Slc33a1* KO PDAC cells generated from WT PDAC cells (**Figure S10A**) would also be sensitized to mmeso CAR T-cell therapy. We injected either 600,000 control KO (IGS_104) or *Slc33a1* KO PDAC cells orthotopically into C57BL/6 mice and treated them with murine control (EGFRvIII) or mmeso CAR T-cells four days later. Consistent with our results, we observed a modest but statistically significant extension in the survival of mice harboring *Slc33a1* KO tumors compared to control KO tumors treated with mmeso CAR T-cells (**Figure S10B-C**). Furthermore, end-stage tumors isolated from mice injected with *Slc33a1* KO PDAC cells treated with mmeso CAR T-cells were also significantly larger than those in all other experimental groups, mirroring all of our previous results with hCD19 CAR T-cells (**Figure S10D**). Thus, *Slc33a1* loss consistently sensitizes PDAC tumors to CAR T-cell therapy.

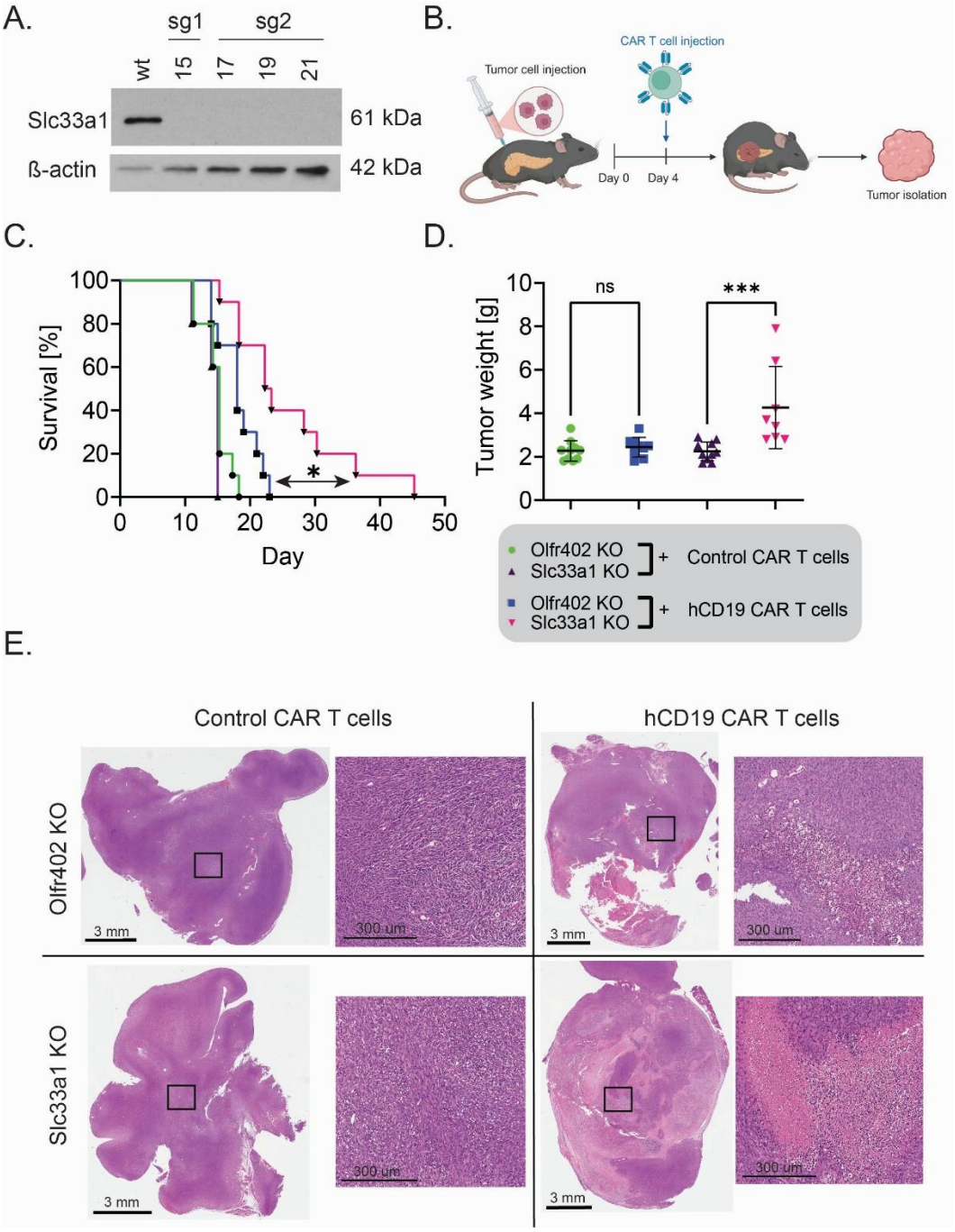

Figure 3: Loss of *Slc33a1* sensitizes to CAR T-cell therapy *in vivo*. A) Western blot analysis showing knock-out of *Slc33a1* in multiple hCD19+ PDAC single cell clones using two different sgRNAs. **B)** Experimental schematic: C57BL/6 mice received an orthotopic injection of 600,000 murine PDAC cells with a control KO (*Olfr402*) or *Slc33a1* KO, followed by a subsequent intraperitoneal injection of freshly prepared hCD19 CAR T-cells (5 million) or control irrelevant CAR T-cells four days later (n=10 per experimental group). Mice were monitored until a humane endpoint was reached and their survival was recorded. **C)** A Kaplan-Meier curve showing survival in mice bearing *Slc33a1* KO or control KO tumors treated with control or anti-CD19 CAR-T cells. *Slc33a1* KO in PDAC cells extends survival in C57BL/6 mice in treated with hCD19 CAR T-cell. Mantel-Cox test p=0.0123. **D)** A graph showing PDAC tumor weight at morbidity in mice treated with hCD19 CAR T-cells or control CAR T-cells. PDAC tumors containing *Slc33a1* KO PDAC cells

treated with hCD19 CAR T-cells are significantly larger p=0.0006. Statistical analysis was conducted with Ordinary One-Way ANOVA test (ns > 0.05, * ≤ 0.05, ** p ≤ 0.01, *** p ≤ 0.001, **** p ≤ 0.0001). **E)** H&E-stained sections of tumors containing PDAC cells with control (*Olfr402*) KO or *Slc33a1* KO treated with hCD19 CAR T-cells or control CAR T-cells. The left side of each panel shows the whole tumor cross-section and the right side zooms into a specified tumor area (black square) demarcated on the left side. PDAC tumors containing *Slc33a1* KO PDAC cells treated with hCD19 CAR T-cells show large necrotic areas.

Single cell RNA sequencing of CAR T-cell treated PDAC tumors reveals changes in cellular redox states

Our primary and secondary screens coupled with validation studies of *Sptlc1* and *Slc33a1* across two different CAR T-cell platforms suggest that aberrant metabolic and oxidative cellular pathways, among others, could impact anti-tumor surveillance by CAR T-cells. To more broadly characterize gene expression changes in PDAC cells exposed to CAR T-cell therapy, we performed single cell RNA sequencing (scRNA seq) of orthotopic hCD19+ PDAC tumors treated with control (EGFRvIII) or hCD19 CAR T-cells. For this purpose, we injected 600,000 hCD19+ PDAC cells orthotopically into C57BL/6 mice and treated them with freshly produced murine CAR T-cells four days later (**Figure 4A**). The hCD19+ CAR T-cells produced for this experiment also showed enhanced killing and IFN-γ release compared to control CAR T-cells in an *in vitro* cytotoxicity assay performed in parallel with the tumor studies (**Figure S11A-C**). CAR T-cell-treated tumors were isolated after 10 days for control CAR T-cell-treated mice and after 15 days for hCD19 CAR T-cell-treated mice, at which stage all PDAC tumors had reached a similar weight (**Figure S11D**). Following tumor dissociation into single cells, live cell mixtures were subjected to scRNA-seq. The resulting data were filtered and gene expression data from 20,516 cells was subjected to unsupervised clustering (**Figure S11E; see Methods**). We identified tumor cells by hCD19 and Cas9 expression, and annotated stromal and immune cell clusters using well-established genes and gene signatures, such as *Cd19* for B-cells and *Cd68* for macrophages (**Figure S11F and Figure S12A**). In total, we were able to identify 12 clusters consisting of PDAC cells, cells of the innate and adaptive immune system, including CAR T-cells (*Cd8a* and GFP expression), endothelial cells, pancreatic stellate cells and erythroid cells (**Figure S12B**).

To identify differentially expressed genes between PDAC cells treated with control CAR T-cells compared to hCD19 CAR T-cells, we isolated the 13,410 PDAC cells in our dataset and performed unsupervised clustering and differential gene expression analysis. Furthermore, we identified differences in the abundance of tumor cells in different regions of the 2-dimensional uniform manifold approximation and clustering (UMAP) plots between control and hCD19 CAR T-cell treatment, showing CAR T-cell treatment specific enrichment and depletion of certain tumor cell clusters (**Figure 4B**). To identify biological processes and molecular functions impacted in PDAC cells upon treatment with CAR T-cells, we performed gene ontology (GO) analysis using gProfiler on the top 100 differentially expressed genes between hCD19 CAR T-cell treated and control CAR T-cell-treated PDAC cells. PDAC cells surviving hCD19 CAR T-cell therapy exhibited downregulation of pathways related to oxidative stress, including glutathione metabolism, oxidoreductase activity, biological oxidation, and the Nrf2 (nuclear factor, erythroid 1-like2) pathway (**Figure 4C**). Conversely, pathways regulating the interaction of tumor cells with the extracellular matrix were overexpressed in hCD19 CAR T-cell treated PDAC cells (**Figure S12C**). Additionally, Gene Set Enrichment Analysis (GSEA) on murine hallmark genes showed that the activity of reactive oxygen species, cholesterol homeostasis, and fatty acid metabolism pathways were reduced in PDAC cells following hCD19 CAR T-cell treatment, while proliferation related pathways such as mitotic spindle assembly, *Kras*, and *Tgf-β* signaling were enriched (**Figure 4D**). Together, these results indicate that PDAC cells treated with hCD19 CAR T-cells exhibit substantial molecular changes in oxidative stress pathways, including the Nrf2 antioxidant response.

The Nrf2-antioxidant response element (ARE) signaling pathway plays a key role in the cellular defense against oxidative or electrophilic stress[62]. The cytosolic protein Kelch-like ECH Associated-Protein 1 (Keap1) acts as the central negative regulator of this pathway by targeting Nrf2 for proteasomal degradation[63]. Intriguingly, mutations in *Keap1* that lead to Nrf2 hyperactivation have been implicated in mediating resistance to immune checkpoint blockade (ICB) therapy in lung adenocarcinoma (LUAD)[64]. To further analyze the connection between the Nrf2 pathway and CAR T-cell therapy, we investigated the expression of a gene signature of murine Nrf2-responsive genes in PDAC cells treated with control CAR T-cells compared to hCD19 CAR T-cells (**Figure 4E, Table S3**).

Consistent with our previous results, expression of murine Nrf2-responsive genes was significantly reduced in PDAC cells that survived hCD19 CAR T-cell treatment compared to control CAR T-cell treatment, leading us to hypothesize that PDAC cells with Nrf2 pathway activation may be preferentially targeted by CAR T-cell therapy.

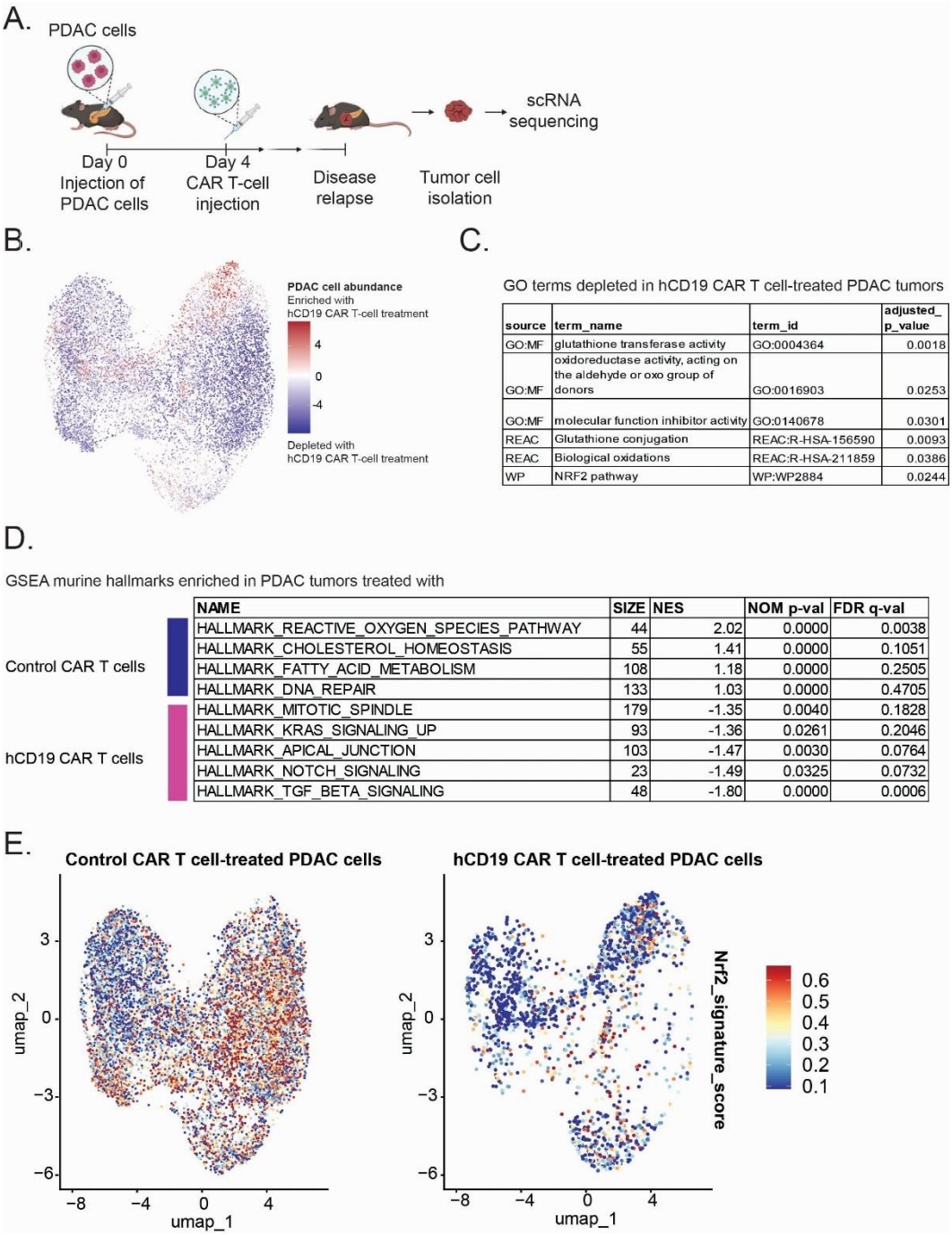

source	term_name	term_id	adjusted_p_value
GO:MF	glutathione transferase activity	GO:0004364	0.0018
GO:MF	oxidoreductase activity, acting on the aldehyde or oxo group of donors	GO:0016903	0.0253
GO:MF	molecular function inhibitor activity	GO:0140678	0.0301
REAC	Glutathione conjugation	REAC:R-HSA-156590	0.0093
REAC	Biological oxidations	REAC:R-HSA-211859	0.0386
WP	NRF2 pathway	WP:WP2884	0.0244

	NAME	SIZE	NES	NOM p-val	FDR q-val
Control CAR T cells	HALLMARK_REACTIVE_OXYGEN_SPECIES_PATHWAY	44	2.02	0.0000	0.0038
	HALLMARK_CHOLESTEROL_HOMEOSTASIS	55	1.41	0.0000	0.1051
	HALLMARK_FATTY_ACID_METABOLISM	108	1.18	0.0000	0.2505
	HALLMARK_DNA_REPAIR	133	1.03	0.0000	0.4705
hCD19 CAR T cells	HALLMARK_MITOTIC_SPINDLE	179	-1.35	0.0040	0.1828
	HALLMARK_KRAS_SIGNALING_UP	93	-1.36	0.0261	0.2046
	HALLMARK_APICAL_JUNCTION	103	-1.47	0.0030	0.0764
	HALLMARK_NOTCH_SIGNALING	23	-1.49	0.0325	0.0732
	HALLMARK_TGF_BETA_SIGNALING	48	-1.80	0.0000	0.0006

Figure 4: Single cell RNA sequencing of CAR T-cell treated PDAC tumors reveals changes in cellular redox states. A) Experimental schematic: C57BL/6 mice received an orthotopic injection of 600,000 murine

PDAC cells, followed by a subsequent intraperitoneal injection of freshly prepared hCD19 CAR T-cells (n=4; 2.5 million) or control irrelevant CAR T-cells (n=4) four days later. PDAC tumors were harvested once tumors reached approx. 1500 mm^3 (day 10 for control CAR T-cell treated tumor; day 15 for hCD19 CAR T-cell treated tumors). Tumors were dissociated into single cell suspensions and chromium single cell RNA sequencing (10x genomics) was performed. **B)** A UMAP of PDAC cells from tumors treated with hCD19 CAR T-cells or control CAR T-cells. The differential abundance of tumor cells between treatment conditions is depicted by color in the UMAP. Tumor cells enriching with hCD19 CAR T-cell treatment compared to control CAR T-cell treatment are colored in red, and tumor cells depleting following hCD19 CAR T-cell treatment are colored in blue. Differentially expressed genes were identified between PDAC cells of these two experimental conditions and used for pathway analyses. **C)** Gene ontology (GO) analysis of top 100 depleted genes in hCD19 CAR T-cell treated tumors compared to control CAR T-cell treated tumors. **D)** Gene Set Enrichment Analysis (GSEA) of murine hallmarks in PDAC cells in hCD19 CAR T-cell treated tumors compared to control CAR T-cell treated tumors. **E)** A UMAP showing the expression of a Nrf2-responsive gene signature (murine orthologs of the human NRF2 Wikipathway) in PDAC cells from tumors treated with hCD19 CAR T-cells or control CAR T-cells. Nrf2-responsive gene expression is lower in PDAC cells treated with hCD19 CAR T-cells compared to control CAR T-cell treated PDAC cells.

Nrf2 hyperactivation sensitizes PDAC tumors to CAR T-cell therapy *in vivo*

To test the hypothesis that PDAC cells with high Nrf2 activation show increased sensitivity to CAR T-cell treatment, we leveraged a previously described *Nrf2* 8xARE-GFP reporter for which GFP expression serves as a readout of *Nrf2* transcriptional activity[65]. Following transduction of WT PDAC cells with the *Nrf2* 8xARE-GFP reporter (*Nrf2* reporter), we validated reporter activity by treating these cells with tert-butylhydroquinone (tBHQ), an established *Nrf2* activator[66]. We observed a robust, dose-dependent induction of GFP expression *in vitro*, thereby validating the assay (**Figure S13A-B**). Next, we orthotopically transplanted 600,000 *Nrf2* reporter PDAC cells into C57BL/6 mice and treated them with either 5 million freshly produced control (EGFRvIII) or mmeso CAR T-cells four days later (**Figure 5A**). Ten days later, we isolated the tumors and analyzed *Nrf2* reporter activity via GFP expression in PDAC cells. Strikingly, *Nrf2* reporter activity was significantly lower in PDAC cells isolated from tumors treated with mmeso CAR T-cells compared to those isolated from tumors treated with control CAR T-cells (**Figure 5B**). These results indicate that PDAC cells with high *Nrf2* pathway activity may be hypersensitive to, and selectively eliminated by, CAR T-cell therapy *in vivo*.

Nrf2 hyperactivation is observed in more than 93% of PDAC and can be triggered by several factors, including oxidative stress, exposure to xenobiotics, and certain cancer-associated mutations[67]. In LUAD, mutations in *Keap1* that lead to Nrf2 hyperactivation

unleash a synthetical lethal interaction with loss of *Slc33a1* due to the increased dependency of *Keap1* mutant cancer cells on ER stress pathways[61]. We confirmed the synthetic lethal interaction between *Slc33a1* KO and *Keap1* KO in hCD19+ PDAC cells using *in vitro* competition assays with hCD19+ PDAC cells containing a control KO (*Olfr402*), *Slc33a1* KO, or *Slc33a1* re-expression in combination with *Keap1* KO. PDAC cells with *Slc33a1*/*Keap1* double-KO depleted over time compared to PDAC cells with single *Slc33a1* KO (**Figure S13C**). In contrast, *Olfr402/Keap1* double-KO cells did not deplete in comparison to *Olfr402* KO PDAC cells. Similarly, *Keap1* KO PDAC cells with restored expression of *Slc33a1* did not deplete. At the experimental endpoint, the remaining PDAC cells in the *Keap1/Slc33a1* double-KO population had selected against *Keap1* loss (**Figure S13D**). These results demonstrate that the *Keap1*/*Slc33a1* synthetic lethal interaction is conserved across different types of tumor cells.

Given that (1) Nrf2-high PDAC cells may be selectively sensitive to CAR T-cells, (2) *Keap1* is a negative regulator of *Nrf2* response, and (3) there is a conserved genetic link between *Slc33a1* and *Keap1*, we tested the mechanistic hypothesis that *Keap1* loss alone could sensitize PDAC cells to CAR T-cell therapy. To test this, we orthotopically transplanted 600,000 hCD19+ PDAC cells with control (*Olfr402*) or previously generated *Keap1* KO (sg2) into C57BL/6 mice and treated them with 5 million control (EGFRvIII) or hCD19 CAR T-cells four days later (**Figure 5C**). Consistent with our hypothesis, mice harboring *Keap1* KO PDAC tumors treated with hCD19 CAR T-cells showed a significant survival advantage compared to mice with control PDAC tumors treated with hCD19 CAR T-cells (p=0.0086; **Figure 5D**). Of note, while *Keap1*-targeting sgRNAs were not present in our initial screening library, the genetic interaction between *Keap1* and *Slc33a1* allowed us to identify a human cancer gene and a mechanistic cellular redox state that modulates response to CAR T-cell therapy.

Loss-of-function mutations in *Keap1* are observed in *KRAS*-driven malignancies, including in LUAD and PDAC[68], prompting us to hypothesize that patient-derived mutations could also sensitize tumors to CAR T-cell therapy. To test this hypothesis, we used base editing to engineer the tumor-derived *Keap1* R470H mutation in WT PDAC cells (**Figure 5E**). Next, we orthotopically transplanted 600,000 WT or *Keap1 R470H/*

R470H PDAC cells followed by treatment with 2 million mmeso or control CAR T-cells four days later. Consistent with our hypothesis, we observed significant survival extension in mice harboring *Keap1 R470H/ R470H* PDAC tumors compared to non-mutant PDAC tumors treated with mmeso CAR T-cells (p=0.0277; **Figure 5F**). These results show that human tumor-derived *Keap1* mutations can sensitize tumors to CAR T-cell therapy.

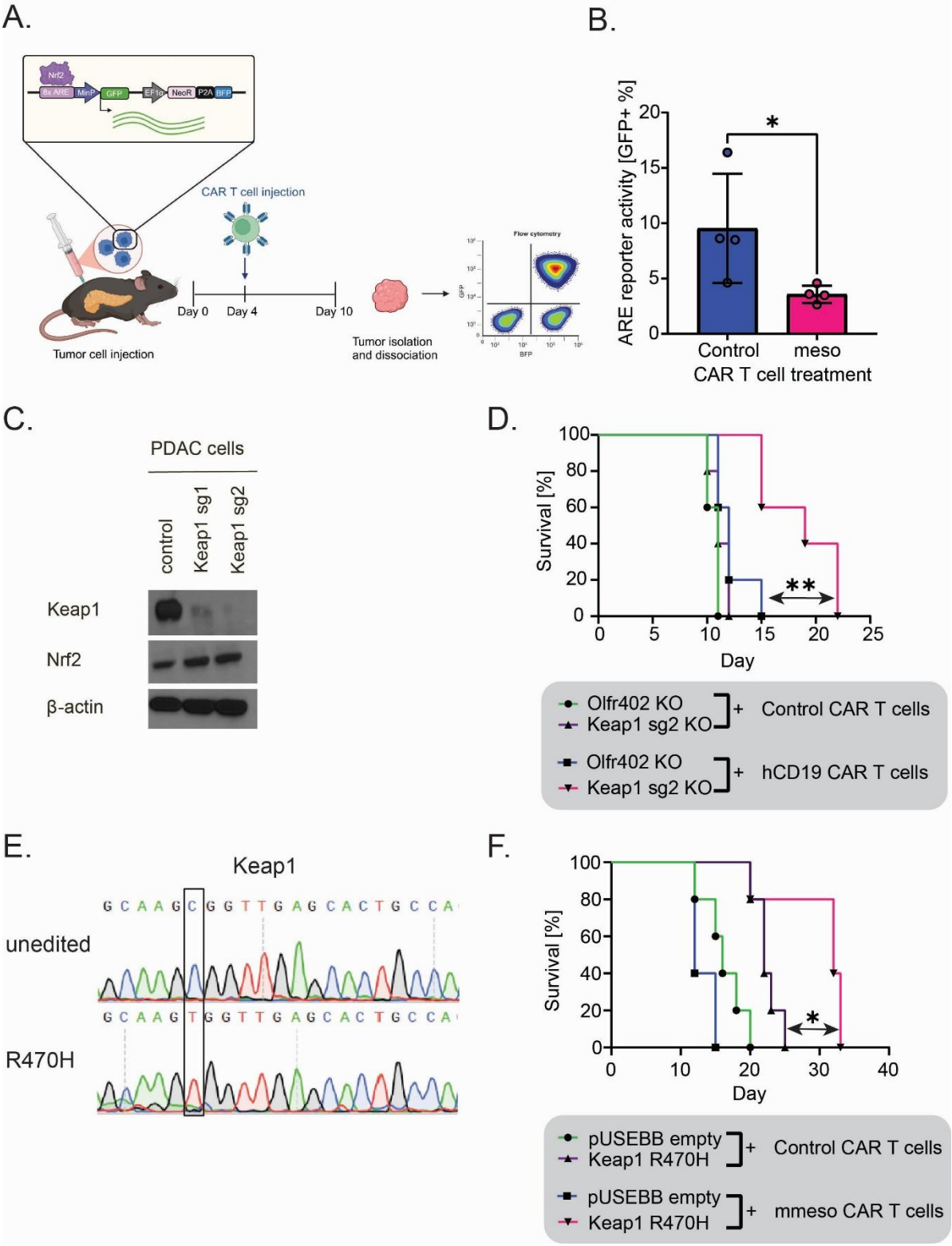

Figure 5: Nrf2 hyperactivation sensitizes to CAR T-cell therapy *in vivo*. A) Experimental schematic: C57BL/6 mice received an orthotopic injection of 600,000 murine PDAC cells expressing a *Nrf2* 8xARE-GFP reporter, followed by a subsequent intraperitoneal injection of freshly prepared mmeso CAR T-cells (5 million) or control irrelevant CAR T-cells four days later (n=5 per experimental group). Binding of Nrf2 to

the ARE sites of the reporter leads to the expression of GFP. Tumors were isolated on day 10 and dissociated into single cell suspensions, and Nrf2 activity (GFP) in PDAC cells (BFP+) was analyzed using a flow cytometer. **B)** A bar graph showing Nrf2 activity (as measured by GFP expression) in PDAC cell isolated from tumors treated with mmeso CAR T-cells compared to control CAR T-cell treated tumors. Statistical analysis was conducted using a Mann-Whitney test (p=0.0286). **C)** Western blot analysis showing *Keap1* levels using two separate sgRNAs in a bulk population of murine PDAC cells. **D)** A Kaplan-Meier curve showing survival of mice bearing Keap1 KO or control PDAC tumors treated with control or anti-CD19 CAR-T cells. C57BL/6 mice received an orthotopic injection of 600,000 murine PDAC cells with a control (Olfr402) KO or *Keap1* KO, followed by a subsequent intraperitoneal injection of freshly prepared hCD19 CAR T-cells (5 million) or control CAR T-cells four days later (n=5 per experimental group). Mice were monitored until a humane endpoint was reached and their survival was recorded. Survival of mice injected with murine PDAC cells with control (Olfr402) KO or *Keap1* KO (sg2) shows that *Keap1* loss significantly extends survival in combination with hCD19 CAR T-cell treatment (Mantel-Cox test p=0.0086). **E)** Sequencing plot showing the *Keap1* loss-of-function mutation R470H that was engineered in PDAC cells using base editing. The sequence of unedited PDAC cells (top) is shown in comparison to the sequence of a single cell clone with a homozygous R470H mutation (bottom). **F)** A Kaplan-Meier curve showing survival of mice bearing Keap1 R470H or control infected PDAC tumors treated with control or anti-mmeso CAR-T cells. C57BL/6 mice received an orthotopic injection of 600,000 murine PDAC cells with or without *Keap1* loss-of-function mutation (R470H), followed by a subsequent intraperitoneal injection of freshly prepared meso CAR T-cells (2 million) or control CAR T-cells four days later (n=5 per experimental group). Mice were monitored until a humane endpoint was reached and their survival was recorded. *Keap1* mutation significantly extends survival in combination with mmeso CAR T-cell treatment (Mantel-Cox test p=0.0277).

Discussion

CAR T-cell therapies have shown limited success in PDAC clinical trials for reasons that remain poorly understood. Importantly, CAR T-cell failure alone is not sufficient to explain the resistance of PDAC to this therapy, suggesting that tumor-intrinsic factors may also be important. Efforts to discover tumor-intrinsic mechanisms of resistance have been hampered by the lack of faithful pre-clinical model systems that are amenable to high-throughput genetic screens. Especially challenging are large scale CRISPR-Cas9 KO screens in PDAC models *in vivo* due to limited orthotopic engraftment rates which do not achieve appropriate sgRNA representation required for screening genome-scale CRISPR libraries. As such, *in vivo* screens in PDAC models published to date often used small libraries, have rarely been performed in orthotopic allografts, and mainly focused on the discovery of genes essential for PDAC growth[69–71]. Multiple *in vivo* screens have sought to identify genes mediating general immune evasion in PDAC and have highlighted a role for antigen presentation, IFN-γ pathway signaling and lipid metabolism[25,49]. Screening for CAR T-cell response modulators in other tumor models has revealed roles for antigen loss[19–21], impaired death receptor signaling in tumor cells[22], and alterations in the IFN-γ

pathway[23–26]. However, to date, no *in vivo* screens for mediators of CAR T-cell response have been performed in solid tumors, including PDAC models.

Here, we established a fully immunocompetent, orthotopic PDAC model that can be used for multiplexed *in vivo* for CRISPR screens in tumor cells to discover and validate mediators of resistance to CAR T-cell therapy. We used of a modular CRISPR library that is divided into individual, non-redundant pools[23], enabling us to perform iterative screening of more than one third of the protein-coding genome and all KEGG pathway associated genes. Using this large-scale screening approach allowed us to uncover hereto unknown mediators of CAR T-cell response, such as sphingolipid enzyme subunit *Sptlc1* and the acetyl-CoA transporter *Slc33a1*. While this screen did not target all protein-coding genes, we were able to uncover new biological mechanisms and mediators of resistance to CAR T-cell therapy that were not present in our original screens, including *Keap1*.

We discovered that loss of *Sptlc1*, which has recently been shown to mediate immune evasion in Kras-driven cancers[49], also sensitizes to CAR T-cell therapy. To our surprise, *Sptlc1* appears to not only be a general T-cell modulator, but to also modulate CAR T-cell response in the tumor microenvironment. In our model, *Sptlc1* loss in PDAC cells led to an influx of CAR T-cells into tumors that could explain the increase in tumor cell killing. To our knowledge, this represents the first example of a non-antigen related alteration in a tumor cell that alters CAR T-cell recruitment to a tumor site.

We then focused on *Slc33a1*, whose loss we discovered to sensitize PDAC cells to CAR T-cell therapy. Recently, *Slc33a1* loss was shown to mediate a synthetic lethal interaction with *Keap1* in LUADs harboring *Keap1* loss-of-function mutations. Combined inactivation of both *Slc33a1* and *Keap1* genes leads to increases in oxidative stress, reactive oxygen species (ROS), induction of the unfolded protein response (UPR)[60,61,72]. Under homeostatic conditions, the antioxidant transcription factor Nrf2 is kept inactive by the oxidative stress sensor Keap1 and only gets released upon stress conditions[73–75]. Thus, cells with loss of *Keap1* function are known to experience Nrf2 hyperactivation, resulting in a redox imbalance that can promote tissue injury and cancer progression[76,77].

Our data reinforce the important connection between *Slc33a1* and the Keap1/Nrf2 pathway. Indeed, our PDAC cells showed synthetic lethality when *Slc33a1* KO was combined with *Keap1* loss. Intriguingly, we discovered through gene expression analysis that PDAC cells resistant to CAR T-cell therapy display a distinct metabolic cell state, characterized by reduced Nrf2 pathway activation, oxidative phosphorylation, and ROS signaling. Further experiments revealed that activation of the Keap1/Nrf2pathway alone, either via endogenous activation or artificially through KO of *Keap1*, was sufficient to sensitize PDAC cells to CAR T-cell therapy. Additionally, we show that a patient-relevant mutation in *Keap1* can similarly sensitize PDAC tumors to CAR T-cell treatment. To our knowledge, this is the first cancer-patient derived tumor mutation that sensitizes to CAR T-cell therapy. This prompted us to test the hypothesis that PDAC cells with redox imbalances could be hypersensitive to CAR T-cell killing, and that this effect could be exacerbated upon of *Slc33a1* disruption. Our data supports this.

Intriguingly, *Keap1* loss-of-function mutations have been shown to correlate with resistance to immune checkpoint blockade (ICB) through diminished dendritic cell (DC) and T cell responses[78]. Although both ICB and CAR T-cell therapy fall under the immunotherapy umbrella, the two therapeutic modalities are fundamentally different from each other. ICB relies on antibodies to enhance the endogenous immune response to antigens presented in the major histocompatibility complex I (MHC-I) on tumor cells, a process requiring both DCs and T cells[79]. Indeed, it has recently been suggested that *Keap1*-mutant tumors may require immunoediting, including MHC-I suppression, to form[80]. Thus, *Keap1*-mutant tumors may be more resistant to ICB. In contrast, CAR T-cell therapy does not require antigen presentation by MHC-I, nor the help of additional endogenous immune cell populations to mount an immune response. As such, our results may be reflective of mechanisms that are unique to adoptive cell-based immunotherapy and highlight the power of our modular *in vivo* screening platform to uncover these.

Recently, the concept that tumor cell states can influence therapy response in PDAC has gained significant traction. For example, PDAC cells in the classical epithelial cell state have been shown to drive resistance to *KRAS* inhibitors, yet these cells also show enhanced sensitivity to cytotoxic T-cell killing[31,32]. However, to date no tumor cell states

have been discovered that can influence CAR T-cell therapy response. Our study decisively shows – for the first time – that tumor-intrinsic metabolic cell states can profoundly sensitize cancer cells to CAR T-cell therapy. This cell state is defined by high activity of the NRF2 antioxidant response pathway. Interestingly, cells with high NRF2 activity are spatially located in the core of the tumor—a region harboring hypoxic cancer cells that are difficult to eradicate with standard-of-care chemotherapies due to poor vascularization and highly developed fibrous stroma[81,82]. Here, CAR T-cell treated tumors across two different genotypes and CAR T-cell platforms showed necrosis, hemorrhage and strong immune infiltration, particularly in the tumor cores, combined with progressive tumor growth after CAR T-cell treatment. Interestingly, these features are all reminiscent of pseudoprogression – a phenomenon observed in immunotherapy in the clinic. This suggests that certain areas of tumors may be more susceptible to CAR T-cell therapy. Furthermore, this orthotopic model may provide some mechanistic insight into the basic phenomenon underlying pseudoprogression.

Our data suggest that CAR T-cell sensitive cell states can arise through genetic and non-genetic mechanisms, including *Keap1* mutations and natural PDAC evolution, respectively. Currently, no know tumor-intrinsic mutations, except those present in tumor antigens, are known to modulate the response to CAR T-cell therapy, and we currently lack any tumor biomarkers that predict CAR T-cell response. Here, we show that a perturbation driving PDAC development, evolution, and therapeutic resistance may also lead to a therapeutically exploitable collateral sensitivity to CAR T-cell therapy. Future studies are needed to identify if PDAC patients harboring tumor-intrinsic alterations in the *Keap1/Nrf2* antioxidant pathway are also hypersensitive to CAR T-cell therapy. Additionally, it needs to be tested if other tumor types, such as *Keap1*-mutant LUAD, are also responsive to CAR T-cell therapy. Yet, these findings open the possibility for achieving therapeutic synergy by combining drugs targeting the *Nrf2* antioxidant pathway that could be used in combination with current CAR T-cell therapies to increase their efficacy in PDAC. Alternatively, therapies that drive the phenotypic selection for *Keap1*-mutant cells could be combined in sequence with CAR T-cells that target this nascent vulnerability.

Methods

Cell culture and cell lines. The cell lines utilized in this study comprised murine PDAC cells (kindly provided by the Vander Heiden Laboratory), human embryonic kidney 293T cells (HEK293T) and Platinum-E (Plat-E) retroviral packaging cells. HEK293T cells, acquired from the American Type Culture Collection (ATCC), were sustained in DMEM with L-glutamine and sodium pyruvate (Corning, 10-013-CM), supplemented with 10% FBS. Murine PDAC cells were grown in DMEM with L-glutamine and sodium pyruvate (Corning, 10-013-CM), supplemented with 10% FBS. Plat-E cells were acquired from Cell Biolabs, Inc. and cultured in DMEM with 10% fetal bovine serum (FBS), 1 µg/mL puromycin, 10 µg/mL blasticidin, penicillin and streptomycin. Routine mycoplasma contamination checks were conducted for all cell lines.

Primary murine T cells were procured from mouse spleens and cultured on plates coated with activating antibodies, as described in the CAR-T cell production methods. The T-cell medium consisted of RPMI with L-glutamine (Corning, 10-040-CM), supplemented with 10% FBS, recombinant human IL-2 (rhIL-2, final concentration of 20 ng/mL; Peprotech, Cat# 200-02-1mg), and 2-mercaptoethanol to a final concentration of 0.05 mM (Gibco, 21985023).

Viral supernatant production. Lentiviral supernatant was produced using standard methods. Briefly, HEK293T cells were transfected with lentiviral transfer plasmid and packaging vector (psPAX2, Addgene, 12260 with VSVg envelop plasmid pMD2.G, Addgene, 12259) using Mirus TransIT-LT1 (Mirus, MIR2305) as indicated by the manufacturer. For retroviral supernatant production, Plat-E cells were switched to DMEM + 10% FBS without antibiotics and transfected with retroviral transfer plasmid using Mirus TransIT-LT1 (Mirus, MIR2305) as indicated by the manufacturer. Viral supernatant was collected 48 hours and 72 hours after transfection, passed through a 0.45 µm filter, and stored at 4 °C for a maximum of one day.

CAR-T cell production. Murine CAR T cells were produced as previously described[23]. Briefly, $CD8^+$ T-cells were isolated from the spleens of 14-week-old male or female C57BL/6 mice (Jackson Laboratory) using Miltenyi Biotec CD8a (Ly-2) MicroBeads for mouse (positive selection kit; Miltenyi, 130-117-044) and LS columns (Miltenyi, Cat# 130-042-401) as per the manufacturer's instructions. The isolated T cells were cultured at $1x10^6$ cells/mL on 6-well plates coated with anti-murine CD3e and anti-murine CD28 activating antibodies (Bio X-Cell, BE0001-1 and BE0015-1) in T cell media.

After 24 hours, activated T cells were collected, counted, and resuspended at $0.5x10^6$ in a 50:50 mixture of fresh T cell media with viral supernatant supplemented with protamine sulfate to a final concentration of 10 µg/mL (MS Biomedicals, ICN19472910). The cells were spin-infected at 1000xg for 1.5 hours at 37 °C on new antibody-coated plates. The next day, T cells were again collected, counted, and resuspended at $1x10^6$ cells/mL in fresh T cell media, re-plated on new antibody-coated plates. Lastly, 24 hours later, T cells were collected, counted, and the percentage of CAR^+ (GFP^+) T cells determined by flow cytometry. The desired number of CAR T cells was then prepared for injection by

resuspension in saline and injected via tail vein. Alternatively, T cells were resuspended at this step in T cell media and plated for *in vitro* cytotoxicity assays.

***In vitro* cytotoxicity assay.** Briefly, target cells were counted and co-cultured with or without CAR T cells at specified Effector-to-Target (E:T) ratios, accounting for the CAR-T transduction efficiency, in T cell media. After approximately 24 hours, the cell suspension was subjected to flow cytometry analysis to evaluate live/dead status (via DAPI stain), %hCD19$^+$ cells (anti-human CD19 BV785; BioLegend #), and %CD8$^+$ cells (anti-mouse CD8-PE/Cy7; BioLegend #100722). Flow cytometry was also employed to determine the densities of each cell type (CAR-T, target cell, non-transduced T-cell). The resulting target cell densities in CAR-T-containing wells were normalized to those in control wells, seeded with the same number of target cells but with control CAR-T or non-transduced T cells. All flow cytometry experiments were conducted with a minimum of 10,000 live cells (via DAPI exclusion) and subsequent data analysis.

Interferon gamma release ELISA assay. The enzyme-linked immunosorbent assay (ELISA) followed standard procedures. Briefly, supernatants from *in vitro* CAR-T cytotoxicity assays were collected and centrifuged to eliminate any contaminating cells. The quantification of IFNγ released by CAR T cells in the supernatant was performed using the DuoSet ELISA kit for mouse IFNγ (R&D systems, DY485). Nunc MaxiSorp flat-bottom plates (Thermo Fisher Scientific, 44-2404-21) were employed for the assay, conducted on a Tecan Infinite 200 Pro machine according to the manufacturer's instructions. To maintain the assay within the linear range of the kit, the supernatant was initially diluted at 1:10 in reagent diluent. Subsequently, a minimum of six serial 4-fold dilutions were executed. For each plate, at least one standard curve was generated, and the entire experiment included at least two standard curves, constructed using standard solutions supplied by the manufacturer. The substrate solution used was 1-StepTM Ultra TMB-ELISA (Thermo Fisher Scientific, 34028), and the stop solution employed was 2N sulfuric acid (VWR, BDH7500-1). Bovine serum albumin (BSA; Sigma, A8022-500G) was prepared as a sterile-filtered 5% stock in PBS (Corning, 21-031-CV).

Fluorescence-activated cell sorting and analysis. The BD FortessaII Cell Analyzer in tube or plate reader format, with BD FACSDiva v9.0 software was used for data collection. All flow cytometry experiments were conducted with a minimum of 10,000 live cells (via DAPI exclusion) and subsequent data analysis. Downstream analysis was performed using FlowJo 10.9.0. The BD FACSAria II Cell Sorter was used for cell sorting.

Western blotting. Cells were lysed with RIPA buffer (Boston BioProducts, BP-115) supplemented with 1X protease inhibitor mix (cOmplete EDTA-free, 11873580001, Roche). Protein concentration of cell lysates was determined using Pierce BCA Protein Assay (ThermoFisher Scientific, 23225). Total protein (25-40 µg) was separated on 4-12% Bis-Tris gradient SDS-PAGE gels (Life Technologies) and then transferred to PVDF membranes (IPVH00010, EMD Millipore) for blotting.

Base editing. An sgRNA targeting R470 in *Keap1* was cloned into the pUSEBB backbone[83]. Lentivirus was produced and WT PDAC cells were transduced and sorted for sgRNA expression (BFP+). Next, cells were transduced with a CBE base editing

reporter (mScarlet+), sorted and nucleofected with CBE editor. The CBE base editing sensor is used as a reporter for Cas9 activity, with successful base editing leading to GFP expression. After 72 hours of recovery, GFP fluorescence was measured via flow cytometry and sorting was used to enrich for base-edited PDAC cells. Next, these cells were single cell-cloned and successful editing was confirmed via Sanger sequencing. A single cell clone with homozygous *Keap1* R470H mutation was used for further experiments.

Ethics statement. The research conducted in this study was conducted ethically and complies with all relevant guidelines and regulations. Animal studies were performed under strict compliance with the Committee of Animal Care (CAC) at the Massachusetts Institute of Technology (protocol number 2402000631).

Animal housing and maintenance. All mouse experiments were conducted under Institutional Animal Care and Use Committee (IACUC)-approved animal protocols at the Massachusetts Institute of Technology (MIT). The mouse strains utilized in this study included C57BL/6 (Jackson Laboratory) and NOD/SCID/IL-2Rg$^{-/-}$ (NSG; The Jackson Laboratories), as indicated in the figure legends. All experimental mice used were 10-16 weeks old. Mice were housed under social conditions (two to five mice per cage) on a 12-hour dark/12-hour light cycle, ambient temperature 21 °C ± 1 °C, and humidity 50% ± 10%. All animals were housed in the pathogen-free animal facility of the MIT Koch Institute, in accordance with the animal care standards of the institutions. Food and water was provided *ad libitum*. All animal research at MIT is conducted under humane conditions with utmost regard for animal welfare. The animal care facility staff is headed by a chief veterinarian and includes a veterinary assistant, animal care technicians, and administrative support. MIT adheres to institutional standards for the humane use and care of animals, which have been established to assure compliance with all applicable federal and state regulations for the purchase, transportation, housing, and research use of animals.

PDAC cell transplantation. PDAC cells were orthotopically injected into the pancreas as previously described[84]. Briefly, PDAC cells were resuspended in HBSS and 600,000 cells in 100 µl were orthotopically injected into the tail of the pancreas using a 26G1/2 needle. Successful injection was confirmed by visible bubble formation in the pancreatic parenchyma. Four days later, mice were intraperitoneally injected with CAR T-cells suspended in saline on the opposing abdominal site.

For experiments in which tumor growth was monitored, mice were imaged every other day using ultrasound. As indicated, tumors were either isolated 10 days after initial injection or mice were closely monitored for signs of disease and distress, and sacrificed upon the appearance of morbidity, in accordance with CAC and DCM policy.

Limiting GFP-dilution assay. 600,000 PDAC cells were orthotopically transplanted into C57BL/6 mice. Five experimental groups of PDAC cells were tested containing diminishing amounts of GFP+ PDAC cells in an RFP+ PDAC cell population: (1) 50% RFP+ and 50% GFP+, (2) 99%RFP+ with 1% GFP+, (3) 99.9% RFP+ with 0.1% GFP+, (4) 99.95% RFP+ with 0.05% GFP+, (5) 99.975% RFP+ with 0.025% GFP+ PDAC cells. Ten days after transplantation, PDAC tumors were isolated and analyzed by flow

cytometry for GFP+ PDAC cells. The recovered percentage of GFP+ cells were then compared to the initial percentage of GFP+ PDAC cells prior to orthotopic transplantation.

Competition assay. For *in vitro* competition assays, PDAC cells with or without hCD19 antigen were mixed at equal ratios and seeded at $1x10^4$ cells per well into a 48-well plate. Next, freshly prepared control (EGFRvIII) or hCD19 CAR T-cells were added at an E:T ratio of 10:1 to the PDAC cells. After approximately 24 hours, the cell suspensions were subjected to flow cytometry analysis to evaluate live/dead status (via DAPI stain), %hCD19$^+$ PDAC cells (GFP+) and %hCD19- PDAC cells (E2-Crimson+). he resulting target cell densities in CAR-T-containing wells were normalized to those in control wells, seeded with the same number of target cells but with control CAR-T or non-transduced T cells.

For *in vivo* competition assays, PDAC cells with or without hCD19 antigen were mixed at equal ratios and 600,000 total PDAC cells were orthotopically transplanted into C57BL/6 mice. Four days later, mice were injected with 2.5 million control (EGFRvIII) or hCD19 CAR T-cells, or with saline as a negative control. Ten days after transplantation, PDAC tumors were isolated and analyzed by flow cytometry. Antigen-negative PDAC cells were identified by E2-Crimson expression and antigen-positive PDAC cells were identified by GFP expression. The ratios of GFP+ to E2-Crimson+ cells were compared between the three experimental groups.

Pooled sgRNA screening. The previously described modular SKY CRISPR library which is divided into 48 individual, non-redundant pools that can be individually screened or combined into larger libraries was used[23]. In this library, Kyoto Encyclopedia of Genes and Genomes (KEGG) protein-coding genes are distributed into pools by pathway ranking, leading to the first 15 pools of the library covering all KEGG pathways. After the first 15 pools, the gene distribution is random. Thus, we elected to screen the first 16 pools of this library in pairs of two to cover all major signaling pathways. To preserve library complexity, a minimum of 1000-fold coverage of the sgRNA library was maintained at each *in vitro* step before the screen, and at a minimum of 150-fold coverage was maintained in all screens completed. Cloned and sequenced plasmid pools, and viral supernatant were generated by the Broad Institute's GPP. For screens, Cas9+ cells were thawed, recovered, and expanded for 5 days to ensure robust growth, and then tested for cutting efficiency to ensure high rates of editing efficiency[85]. In brief, Cas9+ PDAC cells were transduced with the pXPR-047 plasmid that delivers both tdTomato and a sgRNA targeting tdTomato. Thus, active Cas9-expressing lines will result in a reduction in tdTomato over time. After cutting assays were completed, cells were expanded over three additional days and infected with sub-pools. For each of the 16 sub-pools, $6x10^6$ cells were spin-infected with predetermined amounts of viral supernatant such that 30-50% of all cells were infected (expressed E2-Crimson, and survived puromycin selection; MOI«1). Forty-eight hours later, 2 million transduced PDAC cells were started on puromycin selection (5 µg/ml, Gibco, A1113803). Cells were selected over seven days and allowed to recover for two days. On the day of injection into mice, the appropriate number of infected, selected, and recovered cells were combined so that each screen contained two pools. For each screen, PDAC cells injected into the pancreas of C57BL/6 mice as described under PDAC cell transplantation section of this manuscript. On the same day as the injection, input samples were collected. Four days later, 2.5 million

control (EGFRvIII) or hCD19 CAR-T cells were adoptively transplanted into mice via intraperitoneal injection. Mice were sacrificed upon relapse and their tumors were isolated and dissociated into single cell suspensions. For this purpose, tumors were minced with a scalpel and incubated for 30 min in a HBSS-based digestion buffer containing 10 mM HEPES (Invitrogen, #15630080), 12.5U Collagenase IV (Millipore Sigma, C2674), and 200U DNaseI (NEB, #M0303) at 37°C. Next, tumors were further dissociated using a gentleMACS tissue dissociator (Miltenyi Biotec). Enzyme-activity was quenched with FBS and the samples were filtered through sequential filtering steps to obtain single cell solutions. Finally, gDNA from all cells was isolated using the Machery Nagel L Midi NucleoSpin Blood Kit (Clontech, 740954.20). Modifications to the manufacturer's instructions were added as follows: in step1, cells were lysed in the kit's proteinase K containing lysis buffer for longer (overnight at 70 °C). The next morning, lysates were allowed to cool to room temperature, 4.1 µl of RNase A (20 mg/mL; Clontech, 740505) was added, and cells were incubated for 5 minutes at room temperature. The procedure then continued as indicated by the manufacturer. PCR inhibitors were removed from the resulting gDNA (Zymo Research, D6030) and the concentration of the resulting gDNA was measured using the Qubit dsDNA HS assay kit (ThermoFisher, Q32854), and if necessary, diluted to 200 ng/µl with elution buffer. gDNA was then submitted for Illumina sequencing. Data were analyzed as specified in the Data Analysis section of this manuscript.

Single cell transcriptome profiling. C57BL/6 mice were orthotopically injected with $6x10^5$ hCD19+ PDAC cells, followed by intraperitoneal injection with murine CAR-T cells targeting either hCD19 or a control epitope (human EGFRvIII). CAR T-cell treated tumors were isolated after 10 days for control CAR T-cell treated mice and after 15 days for hCD19 CAR T-cell treated mice, at which stage all PDAC tumors had reached a similar weight. Tumors were dissociated into single cells and 10,000 live cells were submitted for transcriptional profiling. Single-cell expression libraries were prepared using the 10x Genomics Chromium v3 reagents. Data were analyzed as specified in the Data Analysis section of this manuscript.

***Nrf2* reporter experiment.** WT PDAC cells were transduced with a previously described *Nrf2* 8xARE-GFP reporter for which GFP expression indicates functional *Nrf2* transcriptional activity[65]. For *in vitro* validation of reporter function, *Nrf2* reporter PDAC cells were treated with tert-butylhydroquinone (tBHQ) and analyzed by flow cytometry for GFP expression 24 hours later. For in vivo experiments, C57BL/6 mice were orthotopically injected with $6x10^5$ *Nrf2* reporter PDAC cells, followed by intraperitoneal injection with murine CAR-T cells targeting either murine mesothelin or a control epitope (human EGFRvIII). CAR T-cell treated tumors were isolated after 10 days, dissociated and PDAC cells (BFP+) were analyzed for GFP expression by flow cytometry.

Tumor histology. PDAC tumors were fixed with 10% Formalin for 24 hours at 4°C and subsequently embedded in paraffin. Tumors were sectioned into 4 µm thick sections and stained with hematoxylin and eosin (H&E). Tumor sections were imaged using an Aperio Digital Pathology Slide scanner (Leica Biosystems) at 20x resolution and analyzed using the corresponding Aperio ImageScope software.

Statistical analysis. All statistical analyses were conducted using GraphPad Prism 10 (GraphPad Software Inc). The specific statistical tests performed for each analysis are outlined in the figure legends. Differences were considered statistically significant for P-values ≤ 0.05.

Antibodies

Western blotting. anti-β-ACTIN (Cell signaling, catalog #4967 S), anti-Cas9 (ActiveMotif, catalog #61577), anti-Sptlc1 (Santa Cruz Biotechnology #sc-374143), anti-Slc33a1 (Millipore-Sigma #WH0009197M7), anti-Nrf2 (Cell Signaling Technology, catalog #12721) , anti-Keap1 (Cell Signaling Technology, catalog #8047) , anti-rabbit IgG HRP-linked antibody (Cell Signaling Technology, catalog #7074), anti-mouse IgG HRP-linked antibody (Cell Signaling Technology, catalog #7076), anti-rat IgG HRP-linked antibody (Cell Signaling Technology, catalog# 7077), Rabbit anti-Armenian Hamster IgG H&L (HRP) (Abcam, catalog #ab5745).

Flow cytometry. anti-human CD19-BV785 (BioLegend, catalog #302240), anti-mouse CD8a-PE/Cy7 (BioLegend, catalog# 100722), and anti-murine CD45-PerCP-Cy5.5 (BioLegend, catalog #103132).

Plasmid constructs:

Plasmid	Producer
psPAX2 (lentiviral packaging)	Addgene plasmid #12260
pMD2.G (VSV-g envelope)	Addgene plasmid #12259
lentiCas9-Blast	Addgene plasmid #52962
hCD19 CAR-P2A-GFP plasmid	Ramos, Koch and Liu et al., Nature Communications, 2023
EGFRvIII CAR-P2A-GFP plasmid	Ramos, Koch and Liu et al. Nature Communications, 2023
pMMLV hCD19(-ICD)	Fröse and Rowley et al., Science Advances, 2024
mmeso CAR-P2A-GFP plasmid	Sequence generously shared by the June lab and then cloned into the same plasmid backbone as other CAR plasmids used in this study.
pRDACrimson_170	Ramos, Koch and Liu et al., Nature Communications, 2023
pXPR-047	Addgene plasmid #107145 with tdTomato instead of eGFP
Nrf2 8xARE-GFP reporter	Zucker et al., Cell, 2025
pLEX307	Addgene plasmid #41392; backbone used for expression of Cas9 resistant Sptlc1 for overexpression
pUSEBB	Sánchez-Rivera and Diaz et al., Nature Biotechnology, 2022

Cytosine base editor (CBE) reporter	Addgene plasmid #136895
Cas9-based CBE editor	Addgene plasmid #215834

CRISPR plasmids. For hit validation, the top 2 scoring sgRNAs for each gene were taken from the SKY library. All other sgRNAs were designed using the Broad Institute's sgRNADesigner tool (https://portals.broadinstitute.org/gppx/crispick/public). sgRNAs were cloned into pRDACrimson_170 or pUSEBB to generate KOs of indicated genes.

sgRNA target	Forward sequence 5'->3'	Reverse sequence 5'->3'
Slc33a1 sg1	CACCGGAAAGGGTAACGATTCCCCT	AAACAGGGGAATCGTTACCCTTTCC
Slc33a1 sg2	CACCGATGTTATCCCGGGAAAACGT	AAACACGTTTTCCCGGGATAACATC
Sptlc1 sg1	CACCGCACACTGATCCCATAGTGCT	AAACAGCACTATGGGATCAGTGTGC
Sptlc1 sg2	CACCGTCCTGCGTACTCTAAGAGAG	AAACCTCTCTTAGAGTACGCAGGAC
Keap1 sg1	CACCGCATGTACCAGATTGACAGCG	AAACCGCTGTCAATCTGGTACATGC
Keap1 sg2	CACCGCGCCTCATCTACACAGCGGG	AAACCCCGCTGTGTAGATGAGGCGC
hCD19 sg1	CACCGCCTCAGCCAGGACCTCACCA	AAACTGGTGAGGTCCTGGCTGAGGC
hCD19 sg2	CACCGCTAGGTCCGAAACATTCCAC	AAACGTGGAATGTTTCGGACCTAGC
hCD19 sg3	CACCGCTAGTGGTGAAGGTGGAAGA	AAACTCTTCCACCTTCACCACTAGC
hCD19 sg4	CACCGATGAAAAGCCAGATGGCCAG	AAACCTGGCCATCTGGCTTTTCATC
hCD19 sg5	CACCGGAGCCCCAAGCTGTATGTGT	AAACACACATACAGCTTGGGGCTCC
hCD19 sg6	CACCGAGTCAATGTGGAGGGCAGCG	AAACCGCTGCCCTCCACATTGACTC
Keap1 R470H	CACCGGAAGCGGTTGAGCACTGCCA	AAACTGGCAGTGCTCAACCGCTTCC

Data Analysis

Primary CRISPR-Cas9 KO Screen

Count data was assigned to SKY library barcodes by the Broad Institute's Genomic Perturbation Platform (GPP) using PoolQ (version 3.3.1) from the output of 5 separate sequencing runs. The resulting 24 counts files were manually assembled using Tibco

Spotfire version 11.4.1.16 and R version 4.4.1[86] with tidyverse version 2.0.0[87] and exported to 8 data matrices. Each matrix contains data for a pair of pools of the SKY library and contains sgRNA identifiers, the corresponding gene association for these identifiers and count data for input, EGFRvIII, and CD19 replicates. Interquartile ranges were calculated for each sample and 5 outliers were identified and excluded from analysis, these were: pool 1+2, EGFRvIII replicate 2, pool 3+4 EGFRvIII replicate 5, pool 7+8 CD19 replicate 16, and pool 13+14 replicates CD19 14 and EGFRvIII 3. These count matrices were then used as input for differential comparison with MAGeCK test version 0.5.9.4[37] with the parameters adjust-method fdr, gene-lfc-method median and norm-method control using a list of negative control guides that target intergenic or olfactory gene sequences. After testing, guide and gene-level data results for each experiment and pool were imported, processed and visualized in R using MAGeCKFlute version 2.8.0[88] and tidyverse 2.2.0[87].
Gene and guide-level data were then aggregated into single data frames in order to visualize differential comparisons across the pools. The 16 pools of the SKY library screened in this study contains 29677 guides targeting barcodes. Of these 27705 target a single gene for a total of 7154 screened genes. Genes of interest and those exceeding different log fold change and FDR thresholds were then selected for validation screening.

Validation CRISPR-Cas9 KO Screen
A validation library was prepared consisting of 1960 sgRNAs. These include 376 non-targeting control sgRNAs and sgRNAs that target 328 genes, usually with 6 distinct guides. Differential analysis was performed for validation screen data with MAGeck test in the same way as for the primary screen. All validation screen samples were used in analysis.

Single cell transcriptome profiling. Sequencing data was aligned to the mm10 reference genome and converted to fastq files using bcl2fastq (v2.20.0.422). Cell count matrices were generated using cellranger (v.6.1.1). Matrices were analyzed by Seurat (v4.0.4) for R (v4.0.2). Digital gene expression matrices were filtered on the following criteria to exclude low-quality cells: number of genes detected in each cell **(=**nFeature_RNA >100, <8000), the total number of molecules detected within a cell **(=**nCount_RNA; top 10% removed) and percent mitochondrial reads (=percent.mito; <25%). The data were further filtered to exclude ambient RNA (SoupX) and doublets (DoubletFinder). Next, data from all tumors was combined into a shared data object and was normalized, scaled, and principal component analysis was performed on the scaled data. The standard deviation of principal components was quantified using an elbow plot, and input dimensions for SNN clustering (20) at which standard deviation = 2 was used. SNN clustering was performed to generate UMAP plots (k.param = 20, res = 0.8). Unique markers for each cluster were identified using FindAllMarkers function. Clusters were annotated using a mix of manual annotation based on well-known lineage genes, such as *Cd68* for macrophages, and the Bioconductor package SingleR. Tumor cells were identified by hCD19 and Cas9 expression and subsetted. Following normalization and scaling, principal component analysis was performed on the scaled data. SNN clustering was performed to generate UMAP plots (k.param = 10, res = 0.4). Differential abundance

analysis was performed using MiloR to compare UMAP changes between control and hCD19 CAR T-cell treated PDAC cells[89]. Differentially expressed genes between PDAC cell with control CAR T-cell treatment and PDAC cells with hCD19 CAR T-cell treatment were identified using the FindMarkers function. The top 100 differentially expressed genes were used for GO analysis. A ranked list based on all differentially expressed genes was used for GSEA analysis. For the generation of a murine Nrf2-responsive gene signature, the human NRF2 WikiPathway geneset (species = "human", collection = "C2", subcollection = "CP:WIKIPATHWAYS", geneset= "M39454") was used and murine orthologs to all genes were identified using the “orthologs” function of the R package “Disco” (v 0.6). The resulting gene list was filtered to only contain genes expressed in our PDAC cells. The murine Nrf2-responsive gene signature was then created of the resulting genes using the Seurat function “AddModuleScore” and displayed in a Feature Plot.

References

1. Siegel, R. L., Giaquinto, A. N. & Jemal, A. Cancer statistics, 2024. *CA. Cancer J. Clin.* **74**, 12–49 (2024).

2. Rahib, L. *et al.* Projecting cancer incidence and deaths to 2030: the unexpected burden of thyroid, liver, and pancreas cancers in the United States. *Cancer Res.* **74**, 2913–2921 (2014).

3. Brunner, M. *et al.* Current Clinical Strategies of Pancreatic Cancer Treatment and Open Molecular Questions. *Int. J. Mol. Sci.* **20**, 4543 (2019).

4. Zhang, X., Zhu, L., Zhang, H., Chen, S. & Xiao, Y. CAR-T Cell Therapy in Hematological Malignancies: Current Opportunities and Challenges. *Front. Immunol.* **13**, 927153 (2022).

5. Park, J. H. *et al.* Long-Term Follow-up of CD19 CAR Therapy in Acute Lymphoblastic Leukemia. *N. Engl. J. Med.* **378**, 449–459 (2018).

6. Shah, N. N. *et al.* Long-Term Follow-Up of CD19-CAR T-Cell Therapy in Children and Young Adults With B-ALL. *J. Clin. Oncol. Off. J. Am. Soc. Clin. Oncol.* **39**, 1650–1659 (2021).

7. Akce, M., Zaidi, M. Y., Waller, E. K., El-Rayes, B. F. & Lesinski, G. B. The Potential of CAR T Cell Therapy in Pancreatic Cancer. *Front. Immunol.* **9**, 2166 (2018).

8. Czaplicka, A., Lachota, M., Pączek, L., Zagożdżon, R. & Kaleta, B. Chimeric Antigen Receptor T Cell Therapy for Pancreatic Cancer: A Review of Current Evidence. *Cells* **13**, 101 (2024).

9. Kakarla, S. & Gottschalk, S. CAR T cells for solid tumors: armed and ready to go? *Cancer J. Sudbury Mass* **20**, 151–155 (2014).

10. Drougkas, K. *et al.* Comprehensive clinical evaluation of CAR-T cell immunotherapy for solid tumors: a path moving forward or a dead end? *J. Cancer Res. Clin. Oncol.* **149**, 2709–2734 (2023).

11. Albelda, S. M. CAR T cell therapy for patients with solid tumours: key lessons to learn and unlearn. *Nat. Rev. Clin. Oncol.* **21**, 47–66 (2024).

12. Sterner, R. C. & Sterner, R. M. CAR-T cell therapy: current limitations and potential strategies. *Blood Cancer J.* **11**, 69 (2021).

13. Young, R. M., Engel, N. W., Uslu, U., Wellhausen, N. & June, C. H. Next-Generation CAR T-cell Therapies. *Cancer Discov.* **12**, 1625–1633 (2022).

14. Labanieh, L. & Mackall, C. L. CAR immune cells: design principles, resistance and the next generation. *Nature* **614**, 635–648 (2023).

15. Milone, M. C. *et al.* Engineering-enhanced CAR T cells for improved cancer therapy. *Nat. Cancer* **2**, 780–793 (2021).

16. Rafiq, S., Hackett, C. S. & Brentjens, R. J. Engineering strategies to overcome the current roadblocks in CAR T cell therapy. *Nat. Rev. Clin. Oncol.* **17**, 147–167 (2020).

17. Jain, M. D. *et al.* Tumor interferon signaling and suppressive myeloid cells are associated with CAR T-cell failure in large B-cell lymphoma. *Blood* **137**, 2621–2633 (2021).

18. Kalbasi, A. & Ribas, A. Tumour-intrinsic resistance to immune checkpoint blockade. *Nat. Rev. Immunol.* **20**, 25–39 (2020).

19. Orlando, E. J. *et al.* Genetic mechanisms of target antigen loss in CAR19 therapy of acute lymphoblastic leukemia. *Nat. Med.* **24**, 1504–1506 (2018).

20. Sotillo, E. *et al.* Convergence of Acquired Mutations and Alternative Splicing of CD19 Enables Resistance to CART-19 Immunotherapy. *Cancer Discov.* **5**, 1282–1295 (2015).

21. Braig, F. *et al.* Resistance to anti-CD19/CD3 BiTE in acute lymphoblastic leukemia may be mediated by disrupted CD19 membrane trafficking. *Blood* **129**, 100–104 (2017).

22. Singh, N. *et al.* Impaired Death Receptor Signaling in Leukemia Causes Antigen-Independent Resistance by Inducing CAR T-cell Dysfunction. *Cancer Discov.* **10**, 552–567 (2020).

23. Ramos, A. *et al.* Leukemia-intrinsic determinants of CAR-T response revealed by iterative in vivo genome-wide CRISPR screening. *Nat. Commun.* **14**, 8048 (2023).

24. Boulch, M. *et al.* Tumor-intrinsic sensitivity to the pro-apoptotic effects of IFN-γ is a major determinant of CD4+ CAR T-cell antitumor activity. *Nat. Cancer* **4**, 968–983 (2023).

25. Dubrot, J. *et al.* In vivo CRISPR screens reveal the landscape of immune evasion pathways across cancer. *Nat. Immunol.* **23**, 1495–1506 (2022).

26. Larson, R. C. *et al.* CAR T cell killing requires the IFNγR pathway in solid but not liquid tumours. *Nature* **604**, 563–570 (2022).

27. de Visser, K. E. & Joyce, J. A. The evolving tumor microenvironment: From cancer initiation to metastatic outgrowth. *Cancer Cell* **41**, 374–403 (2023).

28. Raghavan, S. *et al.* Microenvironment drives cell state, plasticity, and drug response in pancreatic cancer. *Cell* **184**, 6119-6137.e26 (2021).

29. Hwang, W. L. *et al.* Single-nucleus and spatial transcriptome profiling of pancreatic cancer identifies multicellular dynamics associated with neoadjuvant treatment. *Nat. Genet.* **54**, 1178–1191 (2022).

30. Pitter, K. L. *et al.* Systematic Comparison of Pancreatic Ductal Adenocarcinoma Models Identifies a Conserved Highly Plastic Basal Cell State. *Cancer Res.* **82**, 3549–3560 (2022).

31. Singhal, A. *et al.* A classical epithelial state drives acute resistance to KRAS inhibition in pancreas cancer. *Cancer Discov.* **14**, 2122–2134 (2024).

32. Gu, Y. *et al.* Genome-wide CRISPR screens define determinants of epithelial-mesenchymal transition mediated immune evasion by pancreatic cancer cells. *Sci. Adv.* **9**, eadf9915 (2023).

33. Hagel, K. R. *et al.* Systematic Interrogation of Tumor Cell Resistance to Chimeric Antigen Receptor T-cell Therapy in Pancreatic Cancer. *Cancer Res.* **83**, 613–625 (2023).

34. Hingorani, S. R. *et al.* Trp53R172H and KrasG12D cooperate to promote chromosomal instability and widely metastatic pancreatic ductal adenocarcinoma in mice. *Cancer Cell* **7**, 469–483 (2005).

35. Doench, J. G. Am I ready for CRISPR? A user's guide to genetic screens. *Nat. Rev. Genet.* **19**, 67–80 (2018).

36. Hart, T. *et al.* Evaluation and Design of Genome-Wide CRISPR/SpCas9 Knockout Screens. *G3 Bethesda Md* **7**, 2719–2727 (2017).

37. Li, W. *et al.* MAGeCK enables robust identification of essential genes from genome-scale CRISPR/Cas9 knockout screens. *Genome Biol.* **15**, 554 (2014).

38. Ying, H. *et al.* Pten is a major tumor suppressor in pancreatic ductal adenocarcinoma and regulates an NF-κB-cytokine network. *Cancer Discov.* **1**, 158–169 (2011).

39. Tu, Q. *et al.* CDKN2B deletion is essential for pancreatic cancer development instead of unmeaningful co-deletion due to juxtaposition to CDKN2A. *Oncogene* **37**, 128–138 (2018).

40. Meril, S. *et al.* Loss of EIF4G2 mediates aggressiveness in distinct human endometrial cancer subpopulations with poor survival outcome in patients. *Oncogene* **43**, 1098–1112 (2024).

41. Harvey, K. F., Zhang, X. & Thomas, D. M. The Hippo pathway and human cancer. *Nat. Rev. Cancer* **13**, 246–257 (2013).

42. Lawson, K. A. *et al.* Functional genomic landscape of cancer-intrinsic evasion of killing by T cells. *Nature* **586**, 120–126 (2020).

43. McMahon, H. T. & Boucrot, E. Molecular mechanism and physiological functions of clathrin-mediated endocytosis. *Nat. Rev. Mol. Cell Biol.* **12**, 517–533 (2011).

44. Monfort, B., Want, K., Gervason, S. & D'Autréaux, B. Recent Advances in the Elucidation of Frataxin Biochemical Function Open Novel Perspectives for the Treatment of Friedreich's Ataxia. *Front. Neurosci.* **16**, 838335 (2022).

45. Dieterich, I. A. *et al.* Acetyl-CoA flux regulates the proteome and acetyl-proteome to maintain intracellular metabolic crosstalk. *Nat. Commun.* **10**, 3929 (2019).

46. Hannun, Y. A. & Obeid, L. M. Sphingolipids and their metabolism in physiology and disease. *Nat. Rev. Mol. Cell Biol.* **19**, 175–191 (2018).

47. Wang, I.-H. *et al.* Mevalonate Pathway Enzyme HMGCS1 Contributes to Gastric Cancer Progression. *Cancers* **12**, 1088 (2020).

48. Ucche, S. & Hayakawa, Y. Immunological Aspects of Cancer Cell Metabolism. *Int. J. Mol. Sci.* **25**, 5288 (2024).

49. Soula, M. *et al.* Glycosphingolipid synthesis mediates immune evasion in KRAS-driven cancer. *Nature* **633**, 451–458 (2024).

50. Jia, W., Gao, Q., Han, A., Zhu, H. & Yu, J. The potential mechanism, recognition and clinical significance of tumor pseudoprogression after immunotherapy. *Cancer Biol. Med.* **16**, 655–670 (2019).

51. Ma, Y., Wang, Q., Dong, Q., Zhan, L. & Zhang, J. How to differentiate pseudoprogression from true progression in cancer patients treated with immunotherapy. *Am. J. Cancer Res.* **9**, 1546–1553 (2019).

52. Zhao, X. *et al.* Pseudoprogression in CAR-T cell therapy for solid tumor: Case report. *Front. Immunol.* **15**, 1504104 (2024).

53. Schnaar, R. L., Sandhoff, R., Tiemeyer, M. & Kinoshita, T. Glycosphingolipids. in *Essentials of Glycobiology* (eds. Varki, A. et al.) (Cold Spring Harbor Laboratory Press, Cold Spring Harbor (NY), 2022).

54. Hassan, R. & Ho, M. Mesothelin targeted cancer immunotherapy. *Eur. J. Cancer Oxf. Engl. 1990* **44**, 46–53 (2008).

55. Morello, A., Sadelain, M. & Adusumilli, P. S. Mesothelin-Targeted CARs: Driving T cells to Solid Tumors. *Cancer Discov.* **6**, 133–146 (2016).

56. Watanabe, K. *et al.* Pancreatic cancer therapy with combined mesothelin-redirected chimeric antigen receptor T cells and cytokine-armed oncolytic adenoviruses. *JCI Insight* **3**, e99573.

57. Jonas, M. C., Pehar, M. & Puglielli, L. AT-1 is the ER membrane acetyl-CoA transporter and is essential for cell viability. *J. Cell Sci.* **123**, 3378–3388 (2010).

58. Farrugia, M. A. & Puglielli, L. Nε-lysine acetylation in the endoplasmic reticulum – a novel cellular mechanism that regulates proteostasis and autophagy. *J. Cell Sci.* **131**, jcs221747 (2018).

59. Zhou, D., Chen, N., Huang, S., Song, C. & Zhang, Z. Mechanistic insights into the acetyl-CoA recognition by SLC33A1. *Cell Discov.* **11**, 1–4 (2025).

60. Cooley, M. M. *et al.* Deficient Endoplasmic Reticulum Acetyl-CoA Import in Pancreatic Acinar Cells Leads to Chronic Pancreatitis. *Cell. Mol. Gastroenterol. Hepatol.* **11**, 725–738 (2021).

61. Romero, R. *et al.* Keap1 mutation renders lung adenocarcinomas dependent on Slc33a1. *Nat. Cancer* **1**, 589–602 (2020).

62. Nguyen, T., Nioi, P. & Pickett, C. B. The Nrf2-Antioxidant Response Element Signaling Pathway and Its Activation by Oxidative Stress. *J. Biol. Chem.* **284**, 13291–13295 (2009).

63. Baird, L. & Yamamoto, M. The Molecular Mechanisms Regulating the KEAP1-NRF2 Pathway. *Mol. Cell. Biol.* **40**, e00099-20 (2020).

64. Zavitsanou, A.-M. *et al.* KEAP1 mutation in lung adenocarcinoma promotes immune evasion and immunotherapy resistance. *Cell Rep.* **42**, 113295 (2023).

65. Zucker, M. *et al.* Pan-cancer analysis of biallelic inactivation in tumor suppressor genes identifies KEAP1 zygosity as a predictive biomarker in lung cancer. *Cell* **188**, 851-867.e17 (2025).

66. Zagorski, J. W. *et al.* The Nrf2 activator, tBHQ, differentially affects early events following stimulation of Jurkat cells. *Toxicol. Sci. Off. J. Soc. Toxicol.* **136**, 63–71 (2013).

67. Dai, B. *et al.* Compound NSC84167 selectively targets NRF2-activated pancreatic cancer by inhibiting asparagine synthesis pathway. *Cell Death Dis.* **12**, 693 (2021).

68. Chen, X., Su, C., Ren, S., Zhou, C. & Jiang, T. Pan-cancer analysis of KEAP1 mutations as biomarkers for immunotherapy outcomes. *Ann. Transl. Med.* **8**, 141 (2020).

69. Martinez, S. *et al.* In vivo CRISPR screens reveal SCAF1 and USP15 as drivers of pancreatic cancer. *Nat. Commun.* **15**, 5266 (2024).

70. Kubota, C. S., Myers, S. L., Seppälä, T. T., Burkhart, R. A. & Espenshade, P. J. In vivo CRISPR screening identifies geranylgeranyl diphosphate as a pancreatic cancer tumor growth dependency. *Mol. Metab.* **85**, 101964 (2024).

71. Biancur, D. E. *et al.* Functional Genomics Identifies Metabolic Vulnerabilities in Pancreatic Cancer. *Cell Metab.* **33**, 199-210.e8 (2021).

72. Peng, Y. *et al.* Deficient Import of Acetyl-CoA into the ER Lumen Causes Neurodegeneration and Propensity to Infections, Inflammation, and Cancer. *J. Neurosci.* **34**, 6772–6789 (2014).

73. Ngo, V. & Duennwald, M. L. Nrf2 and Oxidative Stress: A General Overview of Mechanisms and Implications in Human Disease. *Antioxidants* **11**, 2345 (2022).

74. Kryszczuk, M. & Kowalczuk, O. Significance of NRF2 in physiological and pathological conditions an comprehensive review. *Arch. Biochem. Biophys.* **730**, 109417 (2022).

75. Tonelli, C., Chio, I. I. C. & Tuveson, D. A. Transcriptional Regulation by Nrf2. *Antioxid. Redox Signal.* **29**, 1727–1745 (2018).

76. Romero, R. *et al.* Keap1 loss promotes Kras-driven lung cancer and results in a dependence on glutaminolysis. *Nat. Med.* **23**, 1362–1368 (2017).

77. Fan, R.-F., Tang, K.-K., Wang, Z.-Y. & Wang, L. Persistent activation of Nrf2 promotes a vicious cycle of oxidative stress and autophagy inhibition in cadmium-induced kidney injury. *Toxicology* **464**, 152999 (2021).

78. Zavitsanou, A.-M. *et al.* KEAP1 mutation in lung adenocarcinoma promotes immune evasion and immunotherapy resistance. *Cell Rep.* **42**, 113295 (2023).

79. He, X. & Xu, C. Immune checkpoint signaling and cancer immunotherapy. *Cell Res.* **30**, 660–669 (2020).

80. Baird, L. & Yamamoto, M. Immunoediting of KEAP1-NRF2 mutant tumours is required to circumvent NRF2-mediated immune surveillance. *Redox Biol.* **67**, 102904 (2023).

81. Toth, R. K. & Warfel, N. A. Strange Bedfellows: Nuclear Factor, Erythroid 2-Like 2 (Nrf2) and Hypoxia-Inducible Factor 1 (HIF-1) in Tumor Hypoxia. *Antioxidants* **6**, 27 (2017).

82. Küper, A. *et al.* Overcoming hypoxia-induced resistance of pancreatic and lung tumor cells by disrupting the PERK-NRF2-HIF-axis. *Cell Death Dis.* **12**, 82 (2021).

83. Sánchez-Rivera, F. J. *et al.* Base editing sensor libraries for high-throughput engineering and functional analysis of cancer-associated single nucleotide variants. *Nat. Biotechnol.* **40**, 862–873 (2022).

84. Hotz, H. G. *et al.* An orthotopic nude mouse model for evaluating pathophysiology and therapy of pancreatic cancer. *Pancreas* **26**, e89-98 (2003).

85. Doench, J. G. *et al.* Rational design of highly active sgRNAs for CRISPR-Cas9–mediated gene inactivation. *Nat. Biotechnol.* **32**, 1262–1267 (2014).

86. R Core Team. R: A Language and Environment for Statistical Computing. Vienna, Austria: R Foundation for Statistical Computing. https://www.R-project.org. (2021).

87. Wickham, H. Welcome to the Tidyverse. Journal of Open Source Software 4(43), 1686. https://doi.org/10.21105/joss.01686. (2019).

88. Wang, B. *et al.* Integrative analysis of pooled CRISPR genetic screens using MAGeCKFlute. *Nat. Protoc.* **14**, 756–780 (2019).

89. Dann, E., Henderson, N. C., Teichmann, S. A., Morgan, M. D. & Marioni, J. C. Differential abundance testing on single-cell data using k-nearest neighbor graphs. *Nat. Biotechnol.* **40**, 245–253 (2022).

List of Supplementary Materials

Fig. S1 to S13 for multiple supplementary figures, as well as supplementary tables 1 to 3.

Data availability

All data are available with this manuscript. Single cell RNA sequencing data will be available at GEO (number in progress).

Acknowledgments

We express gratitude to Koch Institute's Robert A. Swanson (1969) Biotechnology Center, particularly the Animal and Preclinical Imaging core and the Flow Cytometry core, for their technical assistance. CAW is partially supported by Cancer Center Support (core) Grant P30-CA14051 from the NCI to the Barbara K. Ostrom (1978) Bioinformatics and Computing Core Facility of the Swanson Biotechnology Center. We thank Professor Carl H. June for generously sharing the murine mesothelin CAR T-cell sequence with us. We also thank Samuel I. Gould for kindly sharing the *Nrf2* 8xARE-GFP reporter with us. We are very grateful to Dr. Allison Lau and Dr. Sharanya Sivanand for sharing PDAC KPC cell lines with us. Lastly, we would like to acknowledge Biorender for experimental layout figures in this manuscript.

Funding

This work was generously supported by the MIT Center for Precision Cancer Medicine, the Ludwig Center at MIT. The work was also supported by the NCI R01CA290400 (M.H.

and T.T.), the Qualcomm Endowed Discretionary Fund, the Donald A (1967) and Glenda Mattes Cancer Fund, and the Koch Institute Support (core) NIH Grant 5P30-CA014051.

Competing interests: The authors declare no competing interests.

Author contributions (CRediT):

 Writing – original draft: Julia Fröse

 Conceptualization: Julia Fröse, Michael Hemann

 Investigation: Julia Fröse, Charles A. Whittaker, Paul Leclerc, Evelyn Chen, Adam Langenbucher, Sean Doherty, Riley D. Hellinger, Daniel Goulet

 Writing – review and editing: Julia Fröse, Charles A. Whittaker, Paul Leclerc, Evelyn Chen, Adam Langenbucher, Riley D. Hellinger, Daniel Goulet, Tuomas Tammela, Michael Hemann

 Methodology: Julia Fröse, Michael Hemann

 Validation: Julia Fröse, Charles A. Whittaker, Paul Leclerc, Evelyn Chen, Sean Doherty, Adam Langenbucher, Michael Hemann, Tuomas Tammela

 Formal analysis: Julia Fröse, Charles A. Whittaker, Paul Leclerc, Evelyn Chen, Adam Langenbucher

 Project administration: Julia Fröse, Michael Hemann

 Visualization: Julia Fröse, Charles A. Whittaker

 Data curation: Julia Fröse

 Funding acquisition: Michael Hemann and Tuomas Tammela

 Supervision: Julia Fröse, Michael Hemann